Geochemistry Geophysics Geosystems G3

Article
Volume 12, Number 6
7 June 2011
Q05S31, doi:10.1029/2010GC003325
ISSN: 1525-2027

Published by AGU and the Geochemical Society

Arc-parallel shear deformation and escape flow in the mantle wedge of the Central America subduction zone: Evidence from *P* wave anisotropy

W. Rabbel
Institute of Geosciences, SFB574, Christian-Albrechts-University, Otto-Hahn-Platz 1, D-24118 Kiel, Germany (wrabbel@geophysik.uni-kiel.de)

I. Koulakov
Institute of Petroleum Geology and Geophysics, SB RAS, Prospekt Akademika Koptuga, 3, Novosibirsk 630090, Russia (koulakoviy@ipgg.nsc.ru)

A. N. Dinc
Institute of Geosciences, SFB574, Christian-Albrechts-University, Otto-Hahn-Platz 1, D-24118 Kiel, Germany

Now at ExxonMobil Exploration Company, 222 Benmar Drive, Houston, Texas 77060, USA (nilay.dinc@exxonmobil.com)

A. Jakovlev
Institute of Petroleum Geology and Geophysics, SB RAS, Prospekt Akademika Koptuga, 3, Novosibirsk 630090, Russia (jakovlevav@ipgg.nsc.ru)

[1] The *P* wave anisotropy of the crust and uppermost mantle has been determined in two separate areas of the continental margin of Central America covering offshore and onshore parts of southern Nicaragua and northern and central Costa Rica. Our study is based on traveltime data from local earthquakes recorded with three combined onshore and offshore seismic networks that had been deployed in three half-year intervals between 2002 and 2006. The *P* wave traveltime data have been tomographically inverted in terms of an elliptical anisotropic *P* wave velocity distribution. In the upper crust beneath Costa Rica, the seismic anisotropy is of the order of 2%–5% and locally strongly variable in orientation corresponding to the complicated tectonic structure. In contrast, the upper mantle beneath both study regions shows stronger anisotropy of the order of 5%–10% and a more coherent orientation of the axis of fast *P* wave velocity that varies systematically on regional scales: The upper mantle of the incoming oceanic plate is characterized by a trench-normal orientation of the fast *P* wave velocity axis presumably corresponding to mineral alignment (lattice preferred orientation LPO) in transport direction. This pattern is corroded in the uppermost part of the subduction zone, possibly by the influence of bending-related trench-parallel faults and serpentinization that can overprint or annihilate the LPO anisotropy. The upper mantle of the overriding plate and mantle wedge shows a clear trench-parallel orientation of the fast *P* wave velocity axis. The anisotropy is stronger in Nicaragua than in southern central Costa Rica (factor of 2 orders of magnitude). The development of a stronger anisotropy in the Nicaragua could be driven by a change in the stress regime from compressional in southern Costa Rica to transpressional in Nicaragua corresponding to a change from near-orthogonal subduction in the SE to oblique subduction and slab retreat in the NW. From a comparison with *S*/*SKS* wave, GPS, and geochemical observations follows that the most likely explanation for the observed pattern of *P* wave anisotropy in the mantle wedge is LPO caused by a trench-parallel shear deformation and/or NW oriented escape flow originating in the compressional zone near the Cocos Ridge collision area.

Components: 14,300 words, 13 figures, 1 table.

Keywords: Central America; P wave anisotropy; escape flow; seismic anisotropy; seismic tomography; subduction.

Index Terms: 7240 Seismology: Subduction zones (1207, 1219, 1240); 7270 Seismology: Tomography (6982, 8180); 8104 Tectonophysics: Continental margins: convergent.

Received 19 August 2010; **Revised** 30 March 2011; **Accepted** 30 March 2011; **Published** 7 June 2011.

Rabbel, W., I. Koulakov, A. N. Dinc, and A. Jakovlev (2011), Arc-parallel shear deformation and escape flow in the mantle wedge of the Central America subduction zone: Evidence from *P* wave anisotropy, *Geochem. Geophys. Geosyst.*, *12*, Q05S31, doi:10.1029/2010GC003325.

Theme: Central American Subduction System

1. Introduction

[2] A major cause of mantle anisotropy is the strain-induced, preferred orientation of mantle minerals, mainly olivine. Because seismic anisotropy can characterize the orientation and depth extent of the mantle strain fields [e.g., *Savage*, 1999] it is an important tool for understanding the mantle dynamics and tectonics of the Earth's interior and, in particular, of subduction zones. Regarding subduction zones we speak in the following of "arc- or trench-parallel seismic anisotropy" if the fast axis of *P* wave velocity or the polarization of the fast (leading) split *S* wave are oriented parallel to the arc or trench.

[3] Numerous results of *SKS* splitting, receiver functions and seismic tomography, providing information on seismic anisotropy in the crust and upper mantle, are presently available for different subduction zones. For the circum-Pacific belt results were recently compiled by *Long and Becker* [2010] for subslab and mantle wedge *S* wave anisotropy. Regarding the mantle wedge this study revealed that nearly half of the considered investigations show a trench-parallel orientation of fast velocities, whereas the remaining cases show complex or trench-normal polarization of the fast split *S* wave. *S* wave splitting was also investigated previously for the northern part of the target areas of the present study. The splitting of *SKS* waves [*Abt et al.*, 2010] and of *S* waves of local earthquakes [*Abt and Fischer*, 2008; *Abt et al.*, 2009] showed consistently an arc-parallel orientation of the leading *S* wave for the onshore fore arc, the arc and the back arc of Nicaragua and northern Costa Rica.

[4] To explain trench-parallel anisotropy in a mantle wedge the following basic situations can be considered:

[5] 1. The first one assumes trench-parallel shearing or flow in the mantle wedge in combination with A-type dislocation creep [e.g., *Zhang and Karato*, 1995]. In this case, the fast direction of the *P* wave velocity is related to the *a* axis of symmetry of olivine that is parallel to the flow direction. For example, in the Chile-Argentina subduction zone trench-parallel anisotropy can be explained by trench-parallel flow in the mantle wedge caused by a variable dip of the slab [*Kneller and van Keken*, 2007]. The same concept was applied to explain trench-parallel flow in the mantle beneath the South American subducting plate [e.g., *Russo and Silver*, 1994; *Anderson et al.*, 2004]. For the Mariana subduction system, similar mechanisms of trench-parallel flows were modeled by *Kneller and van Keken* [2007].

[6] 2. In a setting of slab entrained corner flow, that is where the shear direction (direction of flow) is trench-perpendicular, the development of "unusual" olivine fabrics could explain the presence of trench-parallel anisotropy. These fabrics occur in a low-temperature or high–shear stress environment if the peridotite contains a high amount of H_2O [*Jung and Karato*, 2001]. One of them is a fabric called B type for which the *c* axis is subparallel to the shear direction and the *a* axis is located orthogonally to it within the shear plane. Similar fabrics can also develop in the presence of microscale melt bands [*Holtzman et al.*, 2003].

[7] 3. Whereas situations 1 and 2 rely on lattice preferred orientation (LPO) of minerals as the major cause of seismic mantle anisotropy, it should not be neglected that structural features, such as magma enriched feeder dyke systems an mylonitic shear zones, can lead to significant anisotropy if they are preferably oriented and show a significant contrast in shear moduli. This shape preferred orientation (SPO) anisotropy can occur at seismic wavelengths even if the involved rock units are

intrinsically isotropic [e.g., *Rabbel and Mooney*, 1996, and references therein].

[8] 4. A combination of trench-parallel LPO and SPO anisotropy can be produced by the foundering of lower crustal material into the upper mantle beneath the volcanic arc [*Behn et al.*, 2007]. The resulting flow patterns correspond to inverted plumes, which contain flow components directed radially toward dripping centers in the lower crust and predominantly vertical components in the upper mantle. These patterns are thought to interfere with a background flow of whatever type.

[9] There is a number of other factors that can cause mantle anisotropy of a specific type, and which can interfere with the situations described above. Examples are serpentinized fluid pathways in the cold outermost mantle wedge possibly caused by dewatering of the slab, the serpentine fabric as such, generally more complex flow paths such as toroidal flow caused, by slab tear-off and rollback (for a comprehensive overview of effects see, e.g., *Abt et al.* [2009] and *Long and Becker* [2010, and references therein]) Even the relatively simple 2-D geometry of slab entrained corner flow can develop a complex pattern of fabric and seismic anisotropy depending on the physical conditions, water content and depth considered [*Lassak et al.*, 2006]. Therefore, an assessment of flow in the mantle wedge cannot be based of seismic anisotropy alone but has to consider other constraining observations and model calculations such as GPS deformation measurements or temperature and flow modeling at depth.

[10] Based on the joint consideration of the results of shear wave splitting and geochemistry, *Hoernle et al.* [2008] interpreted the trench-parallel orientation of the leading split *S* wave beneath north Costa Rica and Nicaragua as an indication of an arc-parallel flow in the mantle wedge above the subducting slab. *Hoernle et al.* [2008] associate shear wave splitting and isotope analyses from volcanic front lavas of Central America. They found that isotope ratios (basically $^{143}Nd/^{144}Nd$ and $^{208}Pb/^{204}Pb$) show a nearly linear trend along the arc. This trend could be explained by a spatially gradual mixing of mantle wedge material carrying two different end-member signatures: (1) the hot spot signature of Galapagos entering the mantle wedge in southern Costa Rica and (2) the signature of hydrated oceanic crust such as found offshore Nicaragua. Interpreting this finding as a material transport from SE to NW, they estimated flow rates of 63–190 mm/yr that are comparable to the magnitude of the Cocos Plate motion (~80 mm/yr) [*DeMets et al.*, 1994]. The combination of these observations is a strong evidence of arc-parallel flow in Costa Rica and Nicaragua.

[11] Seismic structure beneath Costa Rica and Nicaragua has been investigated in a number of tomographic studies based on data acquired by several temporary networks [e.g., *Colombo et al.*, 1997; *Protti et al.*, 1999; *Yao et al.*, 1999; *Sallarès et al.*, 2000; *Quintero and Kissling*, 2001; *Husen et al.*, 2003; *Arroyo et al.*, 2009; *Dinc et al.*, 2010, 2011]. Most of the different authors applied independent approaches. Since the results show consistent structural features they can be considered robust. Due to the varying structure of the Wadati-Benioff Zone, the tomographic studies showed variable penetration depths: In Nicaragua the subducting plate could be followed down to a maximum of ~200 km where it shows a dip of 70°. In Costa Rica only depths to ~70 km have been reached up to where the slab dips with 35° to 60° depending on the region. The crust and lithospheric mantle of the overriding plate shows regionally variable velocities which could be associated with major tectonic units and local structure such as subducting seamounts. A pronounced minimum of velocity and increased Vp/Vs ratios are found in southern Nicaragua suggesting a significant hydration of the mantle wedge [*Dinc et al.*, 2010, 2011].

[12] At the same time, the dynamic state of the deep interior is hard to constrain from isotropic models provided by classical tomographic approaches. Therefore, the main purpose of this study is to investigate the *P* wave anisotropy structure in the crust and upper mantle beneath central and north Costa Rica and south Nicaragua using an anisotropic traveltime tomography algorithm (ANITA by *Koulakov et al.* [2009]). The obtained *P* wave velocity anisotropic structure is complementary to the anisotropic information obtained previously from shear wave splitting and covers an investigation area reaching about 100 km further east and south than previous studies [*Hoernle et al.*, 2008; *Abt et al.*, 2010]. Our investigation area extends offshore until the trench and reaches south until where the Cocos Ridge and the continent collide. This collision has been considered as the cause of an arc-parallel escape flow [e.g., *Hoernle et al.*, 2008].

2. Geological Setting

[13] The tectonic setting of Central America is characterized by the subduction of the Cocos Plate beneath the Caribbean Plate (Figure 1). The Cocos

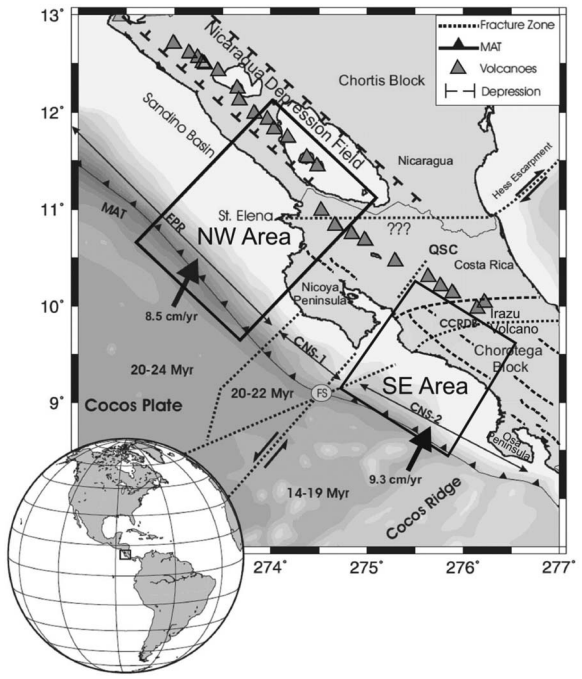

Figure 1. Major geographical and geological units of the study area. Rectangles indicate the two study areas for which the tomographic inversions were performed. CCRDB, Central Costa Rica Deformation Belt; CNS-1, Cocos Nazca Spreading Center 1; CNS-2, Cocos Nazca Spreading Center 2; EPR, East Pacific Rise; MAT, Mid-America Trench; QSC, Quesada Sharp Contortion. Major faults of Costa Rica, along which shear or transpressive movement can take place, are shown as dashed lines [after *Quintero and Güendel*, 2000; *Denyer et al.*, 2003]. From geodetic measurements dextral shear has also been inferred along the volcanic chain in Nicaragua [*DeMets*, 2001]. Plate velocities after *DeMets* [2001].

Plate shows a strong structural variation within relatively short distances. Lateral changes along the volcanic arc of the overriding Caribbean plate have been understood as a consequence of lateral changes in the structure, age and composition of the incoming oceanic Cocos plate [*Carr et al.*, 2007; *Hoernle and Hauff*, 2007; *Barckhausen et al.*, 2001; *Werner et al.*, 1999]. The incoming plate has been divided into three segments based on their morphology [*von Huene et al.*, 1995]: (1) a smooth segment of regular oceanic lithosphere with long trench-parallel fractures off northern Costa Rica (Nicoya Peninsula segment) continuing to Nicaragua, (2) a topographically rough segment covered with seamounts off central Costa Rica (Jaco-Quepos segment), and (3) the thickened and rough oceanic lithosphere of the Cocos Ridge [*Walther*, 2003] subducting beneath southern Costa Rica (Osa Peninsula segment). A corresponding segmentation is found along the arc of the overriding plate: It is volcanically active along the projection of sections 1 and 2 but shows major geochemical differences in the magmas between 1 and 2 [*Carr et al.*, 2003]. Above the subducting Cocos Ridge the Talamanca mountain range formed where the active volcanism stopped in the Late Miocene [*Gräfe*, 1998], showing a recent uplift rate of up to 4.7 mm/yr [*Gardner et al.*, 1992].

[14] The composition and the segmentation of the Cocos Plate have been defined by magnetic anomalies [*Barckhausen et al.*, 2001], multibeam bathymetry [*von Huene et al.*, 1995; *von Huene et al.*, 2000], seismic studies [*Walther*, 2003; *Walther and Flueh*, 2002; *Wilson et al.*, 2003; *Sallarès and Charvis*, 2003; *Sallarès et al.*, 2005] and geological sampling [*Hauff et al.*, 1997; *Werner et al.*, 1999; *Hoernle and Hauff*, 2007; *Wilson et al.*, 2003]. Following these studies, the Cocos Plate is generated at two different zones, the East Pacific Rise (EPR) in the west and the Galapagos Spreading Center (GSC) in the south. The part of the Cocos Plate generated along the EPR subducts beneath Nicaragua and northern Costa Rica. At the trench it is 20–24 Myr old. The part of the Cocos Plate generated at the GSC is 20–22 Myr old where subducting beneath central Costa Rica, and 14–19 Myr old where subducting under southern Costa Rica [*Barckhausen et al.*, 2001].

3. Data and Algorithm

[15] In this paper we consider two neighboring, but not overlapping areas in Central America. The SE area includes two networks, named JACO and QUEPOS, deployed along the Pacific coast of Central Costa Rica from April 2002 to October 2002 and from September 2002 to May 2003, respectively [*Dinc et al.*, 2010]. Here we use the same data as described in detail by *Dinc et al.* [2010] that was used for performing isotropic tomographic inversions. The networks comprised a total of 46 ocean bottom and 27 land stations (Figure 2a). Most of the marine stations were only ocean bottom hydrophones (OBH), 10 of them were equipped with three-component ocean bottom seismometers (OBS).

[16] Another area located to the NW with respect to the first one is covered by an amphibious seismic network which was operated offshore and onshore northern Costa Rica and southern Nicaragua between December 2005 and June 2006 [*Dinc et al.*, 2011]. This network comprises 20 OBS and 30 land seismic stations. Ten of the marine

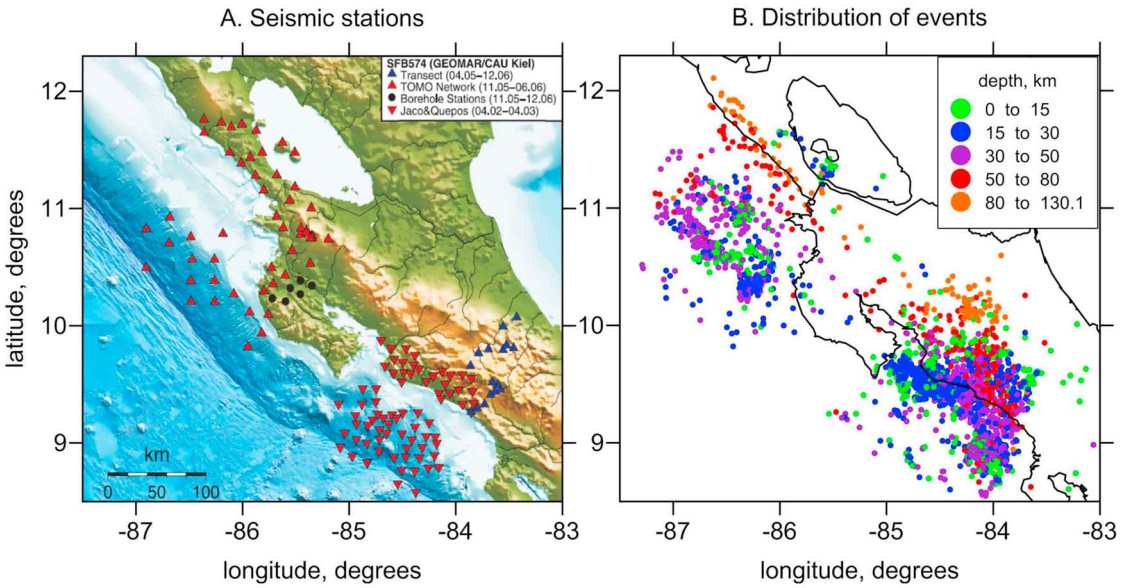

Figure 2. (a) Locations of the two seismic networks the data of which were used in this study. Background is the topography/bathymetry map. The legend indicates the deployment times of the different networks (month/year). (b) Epicenters of the two data sets. Color represents the depths of hypocenters.

stations were only hydrophones and 10 of them were equipped with seismometers (IFM-Geomar type OBS as described by *Bialas and Flueh* [1999]). The land stations were short period Mark-L-3D seismometers with Earth Data Logger (EDL) recorders provided by the geophysical instrument pool of GFZ, Potsdam.

[17] For the tomographic inversion the data set was edited on the basis of a preliminary hypocenter localization with a 1-D velocity model and of the following criteria: (1) each event was observed at a minimum number of 5 stations or more and (2) horizontal distance to the nearest station of the network was <50 km. Applying these criteria, 860 earthquakes of high signal-to-noise ratio with 10770 *P* phase readings were used to perform local earthquake tomography (Figure 2b). The optimum 1-D background models for the both areas were estimated using the VELEST program by *Kissling et al.* [1994].

[18] The processing procedure is based on the anisotropic tomographic code ANITA by *Koulakov et al.* [2009], which was previously used for processing a large data set in Central Java. This code uses first break traveltimes of *P* waves from local events and provides anisotropic *P* wave velocity distributions in 3-D.

[19] One of the most important features of the algorithm is the parameterization of the *P* wave velocity distribution depending on the direction of ray propagation. Considering seismic anisotropy in tomographic traveltime inversion increases the number of unknowns significantly, for example, in case *P* waves in general orthorhombic media by a factor of 9 (6 terms describing the velocity surface and 3 for its orientation in space). This incorporation of more variables can lead to severe conflicts with the numerical stability of the inversion since the conditioning of the tomographic equations is often critical even in the isotropic case, mainly because of restrictions in the source-receiver distribution. In order to find a compromise between stability and information we chose a parameterization with the following simplifications: (1) The *P* wave velocity surface is assumed to be an ellipsoid ("elliptic anisotropy"); (2) the azimuthal orientation of this velocity ellipsoid is variable; but (3) the dip of the velocity ellipsoid is incorporated only in restricted form, namely, "predominantly horizontal" or "predominantly vertical." Our approach leads to a factor of 4 in the number of variables compared to the isotropic case.

[20] Mathematically the chosen velocity surface is represented by an ellipsoid with three orthogonal main axes. One of them is oriented vertically while the other two are oriented arbitrarily in the horizontal plane. An ellipse in the horizontal plain is defined by three parameters $d\sigma_0$, $d\sigma_{60}$, $d\sigma_{120}$, that represent variations of slowness with respect to the reference slowness value, σ_{ref}, along three different

azimuthal directions: 0°, 60° and 120°, respectively. These parameters can be easily converted into three parameters determining the ellipse: maximal, minimal velocities and orientation angle of the main axis. The fourth parameter, $d\sigma_{ver}$, is a slowness variation along the vertical axis. Using these four parameters, slowness along a ray, with the azimuth, α, and dipping angle, β, (measured upward from the vertical axis) can be represented as:

$$\sigma = \sigma_{ref} + (d\sigma_{hor} \sin\beta + d\sigma_{ver} \sin\beta)/(\sin\beta + \cos\beta) \quad (1)$$

where

$$d\sigma_{hor} = d\sigma_1 + d\sigma_2 + d\sigma_3 \quad (2)$$

and

$$d\sigma_1 = d\sigma_0[\cos(2\alpha) + 1]/3$$
$$d\sigma_2 = d\sigma_{60}[\cos(2(\alpha - \pi/3)) + 1]/3$$
$$d\sigma_3 = d\sigma_{120}[\cos(2(\alpha + \pi/3)) + 1]/3$$

[21] In general, the ANITA algorithm uses a similar strategy as the LOTOS code, which is described in detail by *Koulakov* [2009]. The processing starts with the preliminary location of the sources using tabulated traveltimes of a 1-D model. After that, an iterative tomographic procedure starts.

[22] The first step of the iterative inversion procedure is the location of sources in the 3-D anisotropic model. It uses 3-D ray tracing code based on the bending algorithm [*Koulakov*, 2009]. Traveltimes are computed along the ray taking into account a heterogeneous model for the isotropic background velocity and the anisotropy determined in the previous iteration step.

[23] The cell configuration for the velocity parameterization is defined in the first iteration. It is set up by subdividing the study volume into rectangular cells of variable size according to the ray density represented by the cumulative length of all rays crossing a cell normalized to a unit volume. We start from the entire 3-D region and divide it iteratively along the X, Y and Z coordinates. When the normalized cumulative ray length in the actual cell is larger than a predefined value (twice of the average of all cells in this case), it is divided in two equal parts. We stop dividing when a predefined minimum cell size has been reached (5 × 5 × 5 km for Costa Rica and 7 × 7 × 7 km for Nicaragua). Then we remove all cells with a ray coverage lower than a threshold value and the corresponding rays from the inversion. In our case this corresponds to the removal of all cells the diagonal of which is larger than 15 km in central Costa Rica and 25 km southern Nicaragua and northern Costa Rica. The total number of cells was ca. 17000 for the central Costa Rican data set, and ca. 7000 for the southern Nicaragua–northern Costa Rica data set. In Figure 3 we show an example of cell construction. It can be seen that cells are maintained only if they contain segments of the raypaths used in inversion.

[24] In our previous study [*Dinc et al.*, 2010] of the same Costa Rican data set we used a different parameterization method based on nodes connected with each other by tetrahedral cells. The isotropic tomographic velocity anomalies obtained with these two parameterization s are close to identical in both shape and amplitude showing that the solutions are stabile. The ANITA code allows inversion for several differently oriented grids (e.g., for 0°, 22°, 45° and 67° orientations). Averaging the results obtained for different grids decreases the artifacts related to block configuration. For *P* and *S* velocity distributions, the grids are constructed independently.

[25] The calculation of the first derivative matrix representing the effect of velocity variation on the traveltimes of seismic rays is performed numerically along the rays that are computed in the current iteration. If a *P* ray crosses a block we compute four elements of the matrix, which are equal to the traveltime variations of a ray due to the unit variations of each of the four slowness components in this block. For *S* rays we have only one isotropic component per cell. Each line of the matrix contains also four components corresponding to corrections of source coordinates and origin time and station corrections. The ANITA code provides an option for defining both *P* and *S* isotropic models (one parameter per cell in both cases).

[26] The computed first derivative matrix is inverted using a LSQR algorithm [*Paige and Saunders*, 1982; *van der Sluis and van der Vorst*, 1987]. The ANITA code allows controlling weights and damping of different parameters. The smoothness of the model and the anisotropy intensity are tuned by additional matrix blocks which enable Laplacian damping [e.g., *Boschi and Dziewonski*, 1999]. The amplitude damping of the velocity model is controlled by Tikhonov's regularization. These smoothness constraints are realized by additional matrix lines that contain pairs of nonzero elements with values of 1 and −1 linking the velocity components of neighboring cells. The groups of anisotropy parameters assigned to each cell are smoothed in the

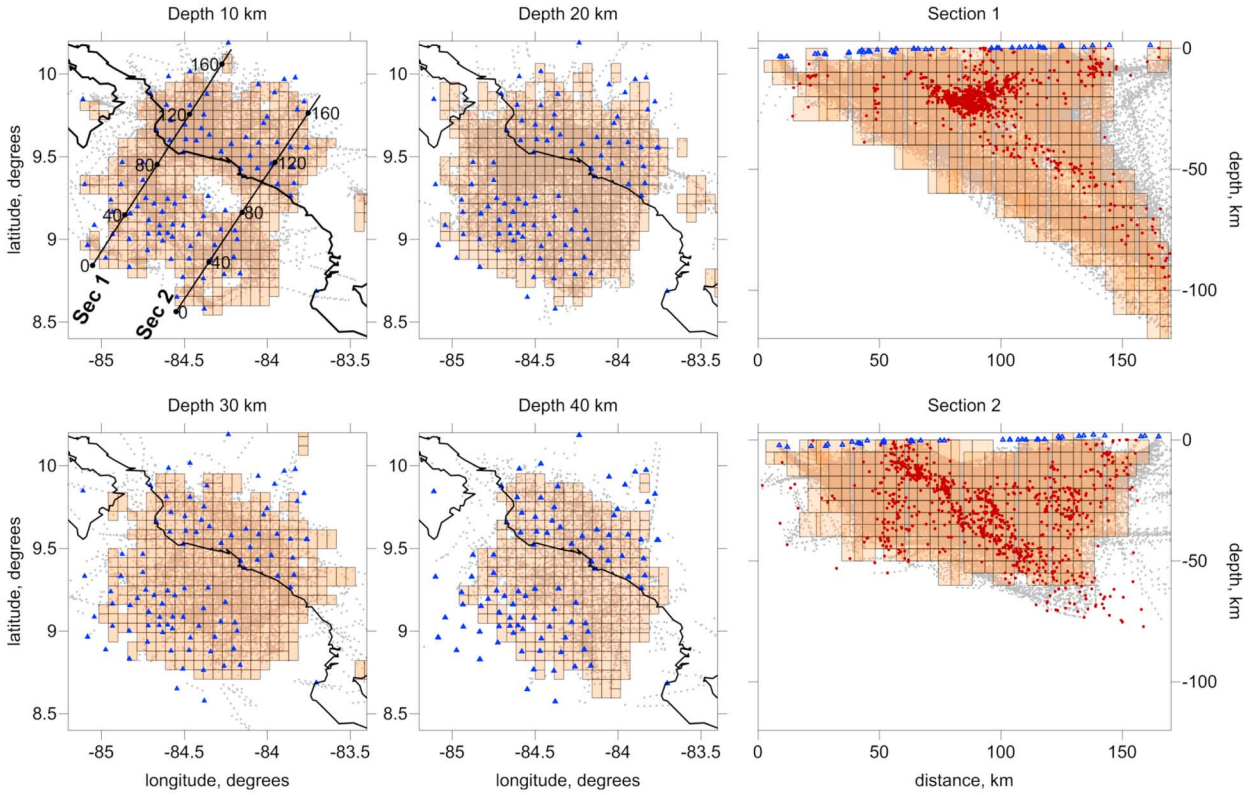

Figure 3. Example of grid construction according to the ray density for the Costa Rica data set. Projections of the raypaths (gray dots) and cells are shown in the vertical and horizontal sections. Triangles show seismic stations, and red dots in the vertical sections are the projections of events located at distances of less than 20 km from the sections. The upper mantle of the downgoing plate ("Sec 1") is sampled by refracted rays traveling updip from the sources at the plate interface.

same way. The general damping of the solution vector is controlled by an additional diagonal matrix block with only one nonzero element in each line and a zero data vector. This corresponds to the standard Marquardt-Levenberg approach. Values of all damping coefficients and weights were chosen on the basis of synthetic modeling using realistic model setup. More details about the tuning of the inversion parameters are given in section 4.4 where the results of synthetic test models are discussed.

[27] After performing the inversion in differently oriented parameterization grids, a summary model is computed in a regular grid by averaging. Then this model is used as a basic velocity distribution in the next iteration that contains the steps of source location in the 3-D anisotropic model of matrix calculation and inversion, as well as computing the summary model in a regular grid. For both study areas 5 iteration steps were applied. The solution were constrained by smoothing coefficients for the isotropic and anisotropic parameters

[28] The ANITA algorithm also provides the possibility of performing the inversion for an isotropic model. In this case it becomes equal to the LOTOS algorithm with cell parameterization. Consequently, isotropic and anisotropic inversions can be combined within one iteration step. In this case the isotropic inversion is performed first, then the time residuals are corrected, and the anisotropic inversion is performed. The resulting model is computed as a sum of isotropic and anisotropic parts. Finding adequate inversion parameters for the isotropic and anisotropic parts of the model is an important and difficult problem in anisotropic tomography. Actually, there is no general criterion for defining the optimal values of the different inversion parameters. We selected these parameters by applying test values to the inversion of synthetic traveltimes for checkerboard and other more realistic underground models. The damping parameters that robustly resolved the realistic synthetic models were then applied to the field data, too. In order to stabilize the results and obtain an optimum resolution of the

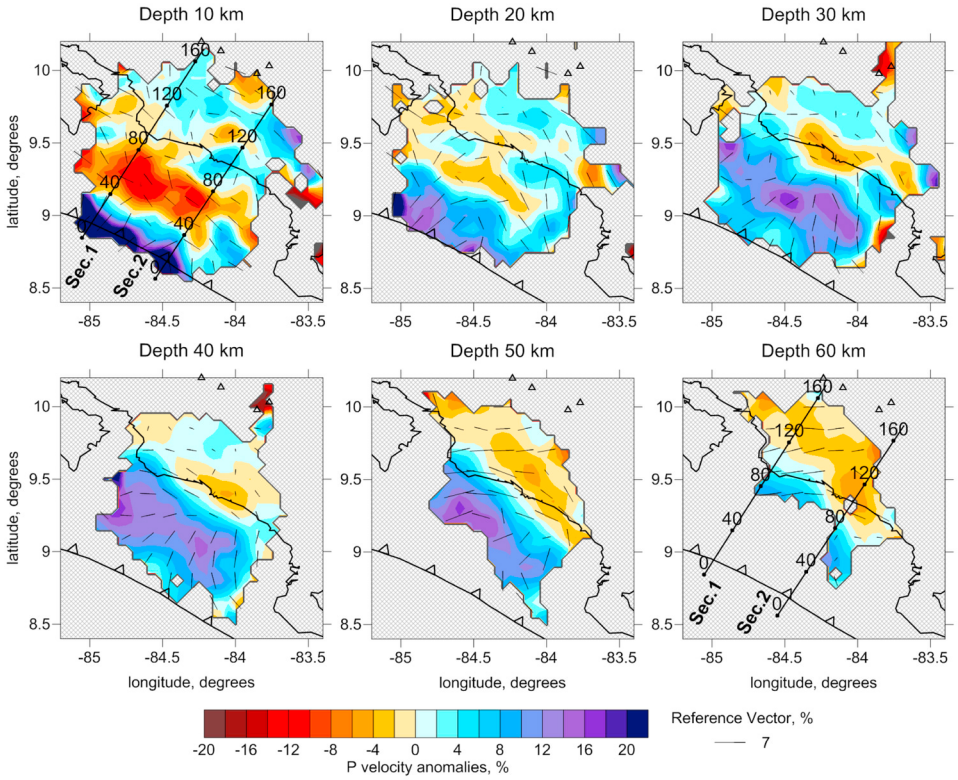

Figure 4. Results of anisotropic *P* wave traveltime inversion in horizontal sections for central Costa Rica. Colors indicate the isotropic velocity perturbations, which are computed as an average of four anisotropic parameters for each point. Bars show the directions of maximum horizontal velocities. Lengths of vectors correspond to the velocity anisotropy in the horizontal direction (equation (3)). A reference vector (7% of anisotropy) is shown in the bottom right corner. The locations of the vertical sections in Figure 5 are shown in the 10 km and 60 km maps.

background structure one has to consider different damping parameters for the isotropic and anisotropic portions of the models. Usually, the anisotropic parts of the solution have to be damped stronger than the isotropic parts.

4. Results and Verification of Anisotropic Inversion

4.1. Presentation of the Results

[29] In sections 4.2 and 4.3 we present the inversion results for two areas in Central America that were obtained independently from each other. In terms of RMS residuals the inversion converged after five iterations (Table 2) each of them containing subsequent isotropic and anisotropic inversions.

[30] As we stated in section 3, in the horizontal plane the elliptical anisotropy distribution is described by three parameters representing slowness variations in three directions. These parameters can be unambiguously converted into the terms dv_{max} and dv_{min} that are the maximum and minimum horizontal velocities and orientation of the fast velocity direction in the horizontal plane. Maximum and minimum velocity anomalies are selected from 180 values computed for all azimuths with 1° step width using equation (2). The anisotropy is shown by bars in the horizontal sections of Figures 4 and 6. The orientation of the bars shows the direction of the main anisotropy axis in which the horizontal velocity is maximal. The length of the bars reflects the magnitude of the anisotropy, which is computed as:

$$A^{hor}(\%) = 100(dv_{max} - dv_{min})/V_{ref} \qquad (3)$$

where V_{ref} is the reference velocity. Orientation and lengths of anisotropy is obtained numerically by calculating the velocity in different directions using formulas (1) and (2) with the step of 1°. The isotropic velocity anomaly is computed as an average of velocity variations in all directions.

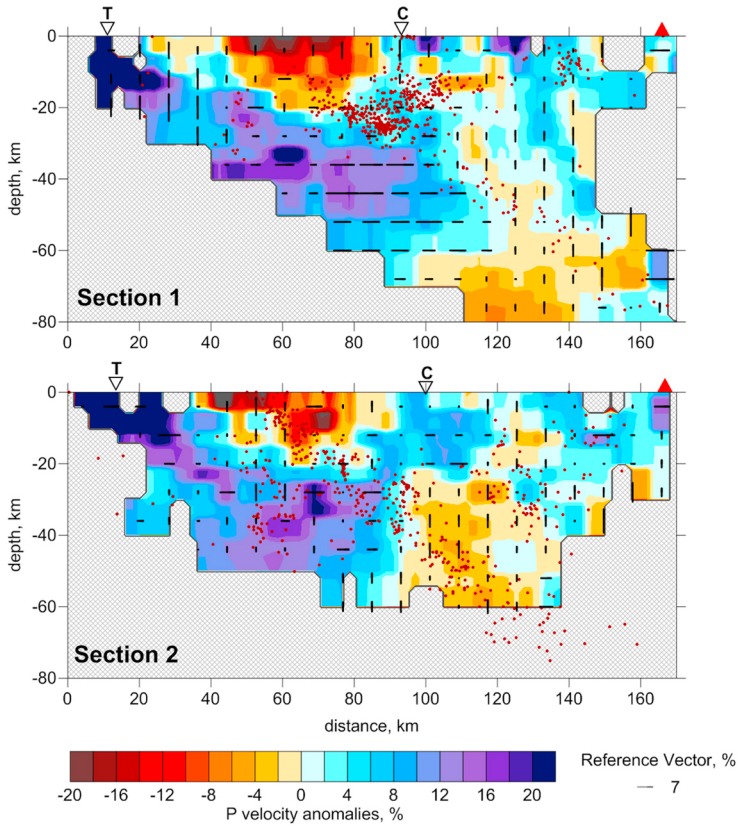

Figure 5. Vertical section of the anisotropic *P* wave velocity model for central Costa Rica. Bars show the difference between average horizontal and vertical velocities. Horizontal (vertical) bars mark the areas with higher horizontal (vertical) velocity; the length of the bars represents the difference between vertical and horizontal velocities. A reference vector (7% of anisotropy) is shown in the bottom right corner. Seismic events located closer than 20 km to the section are shown by brown dots. T and C are the locations of the Trench and the Pacific coast; red triangles show the volcanic arc.

[31] In the vertical sections (Figures 5 and 7), the bars correspond to values of average vertical anisotropy computed by:

$$A^{ver}(\%) = 100(dv_z - dv_{hor})/V_{ref} \quad (4)$$

where dv_{hor} is the average velocity anomaly in the horizontal plane, and dv_z is velocity perturbation along the vertical axis. The bars in the cross section are either vertical if A^{ver} is positive or horizontal if A^{ver} is negative.

[32] In order to assess the significance of the anisotropy we compared the final *P* wave residuals of anisotropic and isotropic inversions. The values of the residuals after each of the five iterations for the two areas are presented in Table 1.

[33] For central Costa Rica the anisotropic inversion leads to a decrease of RMS residuals from 0.150 s to 0.140 s (7.14%). For southern Nicaragua/northern Costa Rica the reduction is higher: from 0.265 s to 0.231 s (14.71%).

4.2. Description of the Results in Central Costa Rica (SE Area)

[34] The resulting anisotropic model for the SE area, central Costa Rica, is presented in four horizontal and one vertical section in Figures 4 and 5. The shapes and amplitudes of the velocity anomalies of the isotropic background model are nearly identical with the isotropic inversion derived by *Dinc et al.* [2010]. Note that two different parameterization algorithms, with nodes and cells, were used in these two cases. It shows that the inversion provides robust images regardless the parameterization method. A detailed discussion of isotropic patterns beneath the SE area is provided by *Dinc et al.* [2010]. Here we shortly repeat the description of the most prominent isotropic structures and then we will focus on new results of anisotropic inversion.

[35] The main feature of the isotropic background model is a clear image of the high-velocity slab. As shown in the vertical section in Figure 5, the upper

Table 1. RMS Values of *P* Wave Traveltime Residuals and RMS Reduction With Respect to the Starting Model for Anisotropic and Isotropic Tomographic Inversion With the ANITA Code

	Anisotropic *P* Model		Isotropic *P* Model		
Iteration	RMS of *P* Residuals (s)	Reduction With Respect to Iteration 1 (%)	RMS of *P* Residuals (s)	Reduction With Respect to Iteration 1 (%)	Additional RMS Reduction due to Anisotropy (%)
			Model 1: South Central Costa Rica		
1	0.309	0	0.309	0	0
2	0.180	41.63	0.190	38.61	5.55
3	0.155	49.96	0.164	46.77	5.80
4	0.146	52.70	0.156	49.53	6.84
5	0.140	54.58	0.150	51.45	7.14
			Model 2: South Nicaragua–North Costa Rica		
1	0.363	0	0.363	0	0
2	0.283	21.98	0.316	12.97	11.66
3	0.252	30.65	0.292	19.55	15.87
4	0.238	34.43	0.278	23.37	16.80
5	0.231	36.34	0.265	27.01	14.71

surface of the slab fits well with the distribution of seismicity and has a dip angle of about 35°. In the mantle wedge, between the subducting slab and continental Moho at about 30 km depth, we observe low-velocity anomalies. The crust seems to be very heterogeneous. A strong low-velocity anomaly is observed beneath the continental shelf (at 40–80 km from the trench), further to the NE we observe a high-velocity anomaly (120–160 km) that can be interpreted as a consolidated fore-arc block. The volcanic arc is located outside but close to NE border of the study area where we observe an inclined low-velocity anomaly at the depths of 30 and 70 km (at 160 km in vertical sections of Figure 5). It can be interpreted as a part of the feeding path between the slab and the volcanoes. However, this anomaly is located near the boundaries of the model where the ray coverage is lower and, therefore, less reliable than in the center.

[36] The new feature of the model is the anisotropic structure shown by bars in the horizontal and vertical sections in Figures 4 and 5. For the shallowest section at 10 km depth we observe a strong variation of the bar orientations. This patchy appearance of the anisotropy can be regarded as an expression of the complex structure of the upper crust. The NW onshore part of the study area belongs to the Central Costa Rica Deformation Belt (CCRDB in Figure 1) that consists mainly of magmatic rocks permeated by complex network of NW and NE trending strike-slip faults and other faults of varying orientation (see, e.g., the tectonic atlas of Costa Rica by *Denyer et al.* [2003]). In the upper crust seismic anisotropy is strongly influenced by the local alignment of fractures [e.g., *Rabbel and Mooney*, 1996, and references therein]. Therefore, complex fault related fracture pattern can be regarded as the most probable cause of the nonuniform appearance of anisotropy in the upper crustal layers. Outside the CCRDB, in the SE of the study area, the upper crustal anisotropy appears more regularly oriented, parallel to the trench, which corresponds to the predominant fault strike in this region.

[37] In the deeper sections the anisotropic structure looks more regular. Beneath the offshore area where the high-velocity anomaly of the slab is detected, we observe an anisotropy of about 7%–10% oriented parallel to the movement of the incoming plate. In the onshore area the anisotropy is weaker (5%–7%) and oriented subparallel to the trench (NW-SE) at 40 km depth, then turning to east-west at 50 to 60 km depth beneath the CCRDB (NW onshore part of the study area). The E-W direction is also the direction along which the CCRDB extends laterally (we avoid to call it "strike direction" because of the complexity of the fault system). Interestingly, the upper mantle shows a positive anomaly of the Vp/Vs ratio beneath the CCRDB [*Dinc et al.*, 2010]. Synthetic tests (section 4.4) show that these zones with different orientations of anisotropy can be reliably separated by our algorithm.

[38] The anisotropy patterns of the vertical section (Figure 5) show only the ratio between horizontal and vertical components of velocity indicated by the orientations of the bars: if the horizontal component is larger than the vertical the bar is horizontal, and vice versa. The true, possibly inclined orientation of the anisotropy ellipsoid cannot be recovered in the vertical plane with the chosen

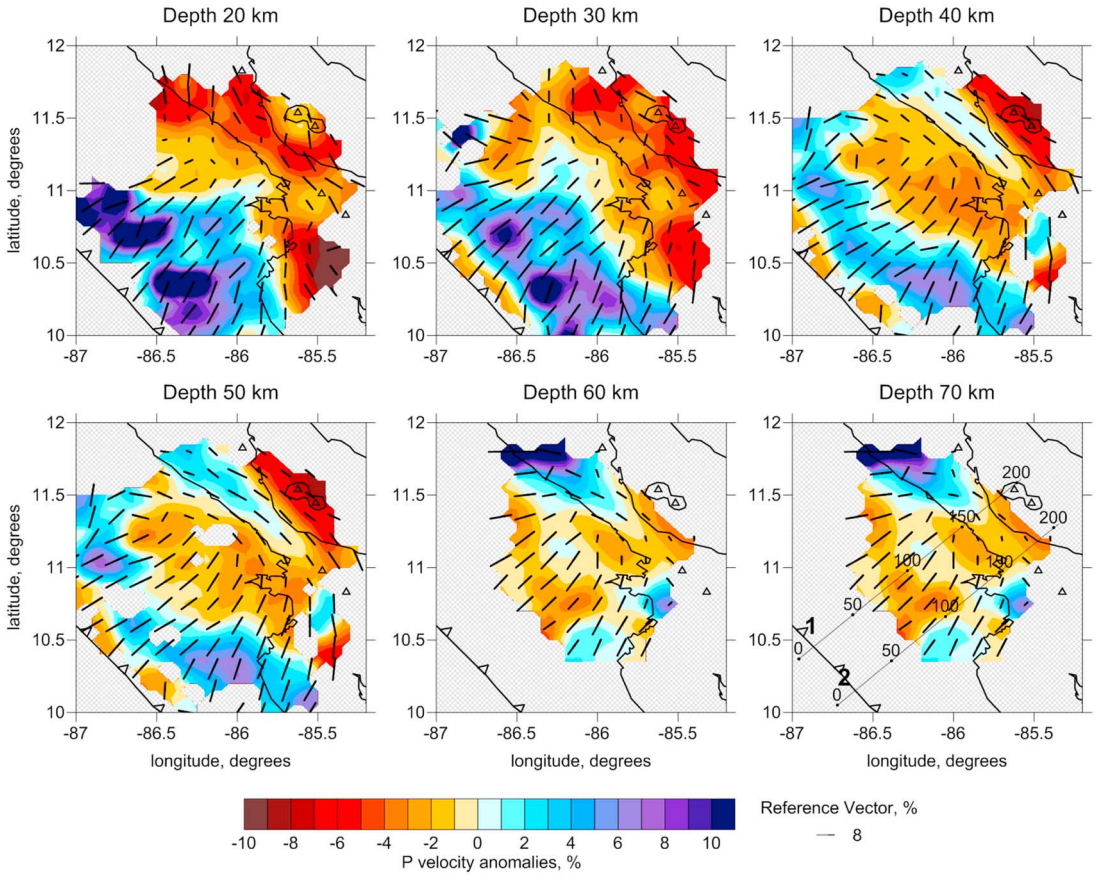

Figure 6. Same as Figure 4 but for the Nicaragua and northern Costa Rica model. The locations of the two vertical sections of Figure 7 are shown in the 70 km map.

parameterization. At the same time, even such a simplified representation showing which of the components, horizontal or vertical, is larger, can be useful in analyzing the results. In the vertical section (Figure 5) we see that the bars are clearly horizontal in the high-velocity part of the slab down to 30 km depth where the dip angle of the slab is smaller than 45°. This result indicates that the horizontal velocity component is higher than the vertical one. In the incoming plate the corresponding azimuth of high *P* wave velocities is very close to the NE direction of plate motion (compare Figure 1 and 4). Therefore, it can be assumed that the underlying anisotropy is caused by the lattice preferred orientation (LPO) of olivine minerals that got oriented by creep parallel to the transport direction of the oceanic plate. The oceanic crust is not resolved in the tomographic images. However, the anisotropy values found near the top of the subducting plate have to be regarded as an average of the properties of the crust and upper mantle. Since the generation and evolution of the oceanic crust are processes that take place in preferred spatial directions, too, it can be assumed that the oceanic crust also contributes to this bulk anisotropy.

[39] Above the subducting plate, the anisotropy bars are shorter, except for two areas where the anisotropy is oriented vertically. One of them is a low-velocity area in the crust at distances of 90–120 km along the profile, where moderate anisotropy (~7%) is oriented vertically. Another pattern is observed in the mantle wedge at depths below 40 km in a distance of ~160 km along profile. Note that a short length of bars in vertical sections does not necessarily mean that the anisotropy is weak. For example, strong anisotropy with dipping angle of 45° would be represented as zero-length bars.

4.3. Description of the Results in Southern Nicaragua and Northern Costa Rica (NW Area)

[40] Here we describe the results from the NW area including southern Nicaragua and northern Costa Rica, for which the resulting horizontal and vertical sections are shown in Figures 6 and 7. The resolved

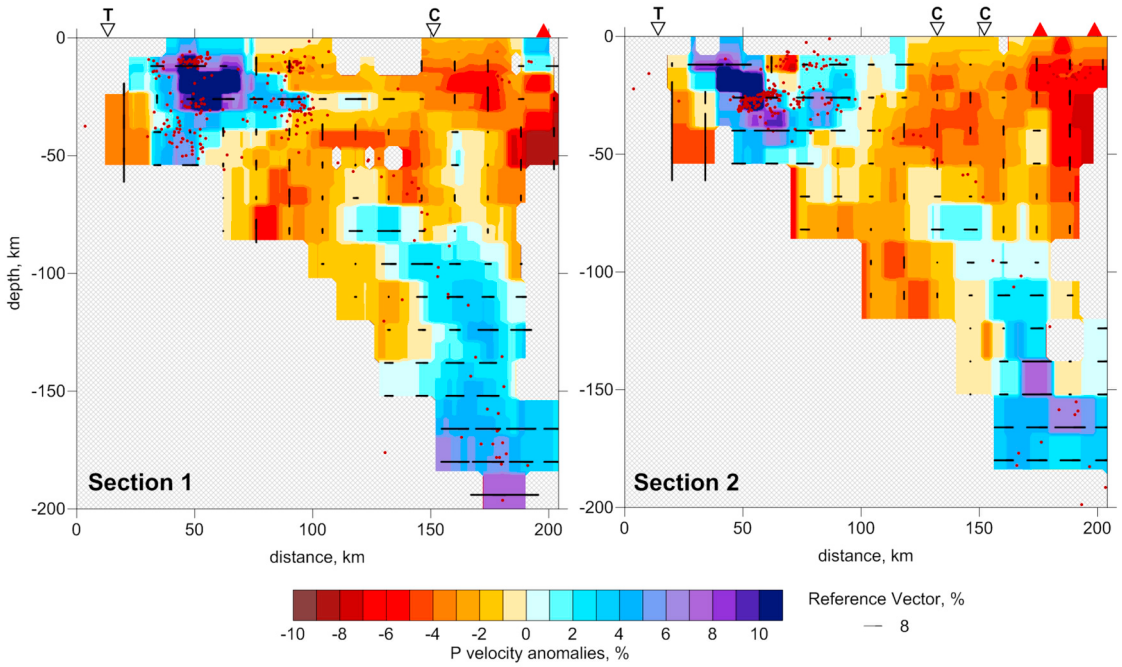

Figure 7. Vertical sections of the Nicaragua and northern Costa Rica model. Horizontal (vertical) bars mark the areas with higher horizontal (vertical) velocity; the length of the bars represents the difference between vertical and horizontal velocities. A reference vector (8% of anisotropy) is shown in the bottom right corner. Seismic events located closer than 20 km to the section are shown by brown dots. T and C show the locations of the trench and the Pacific coast; red triangles depict the locations of the arc volcanoes.

tomographic depth range for this area is much larger than for central Costa Rica because of the occurrence of up to 200 km deep earthquakes within the seismic network.

[41] In the area of southern Nicaragua–northern Costa Rica the cold and dense slab appears as a high-velocity anomaly with a dip angle of 35° in the upper 60 km depth that steepens to ca. 70° down to 200 km depth. The top of the slab is resolved by rays refracted through the upper mantle of the downgoing plate. It coincides with the upper envelope of the earthquake distribution. The dip of the slab gets shallower from north (38°) to south (30°) in the upper 60 km depth. The dip angle does not change significantly in the deeper parts but the number of events decreases in these depths from north to south.

[42] The mantle wedge corner of the overriding plate is found between 30 and 70 km depth at 100 to 150 km distance from the trench. It shows a 4% decreased *P* velocity with respect to 7.9 km/s. This low-velocity zone starts at the mantle wedge corner and continues toward the volcanic arc. The width of the zone is 30 km and the angle to the horizontal is ~15°. At the mantle wedge corner this low-velocity anomaly is associated with an increased Vp/Vs ratio of about 2 [*Dinc et al.*, 2011], which can be seen as an indication of mantle wedge hydration.

[43] The slowest *P* wave velocities of the mantle are found directly beneath the volcanoes from where they extending almost vertically to 100–150 km depth (Figure 7). This low-velocity anomaly is wider in the northern profiles and gets weaker toward the south. Low-velocity zones can be caused by a number of factors such as changes in rock composition, increasing temperature and pore pressure, fracture zones or the presence of pore fluids or partial melting. The observations that the velocity minimum occurs directly beneath the active volcanic arc and that it extends vertically downward make it plausible to associate it with the uprise of fluids and magma from the subducted slab. This view is supported by the enlargement of the velocity minimum from south to north that correlates with an increase in volcanic activity from south to north (an isotropic tomogram of higher resolution is given by *Dinc et al.* [2011]). This volcanic activity has been quantified in terms of

tephra volumes and erupted masses [*Kutterolf et al.*, 2008]. It correlates with volatiles included in the magmas, too [*Sadofsky et al.*, 2008].

[44] As in the case of central Costa Rica, the orientation vectors of fast axis of the anisotropic velocity ellipsoid are aligned perpendicular to the trench in the offshore part of the study area (see map view in Figure 6). Between 85°W and 84°W in central Costa Rica and 86°W and 87°W in southern Nicaragua–northern Costa Rica, the fast horizontal velocity axes are oriented clearly NE-SW, but the directions are rotated to N-S near Osa Peninsula (83.8°W) and near Nicoya Peninsula (85.5°W). Since both peninsulas are near the boundaries of the observation areas the vector orientations are not as reliable as in the central parts but correlate with the recent surface deformation field estimated from GPS observations [cf. *LaFemina et al.*, 2009] and could be real.

[45] Between the coast and the volcanic chain, the fast horizontal velocity directions rotate to arc-parallel onshore along the volcanic chain. Compared to central Costa Rica, southern Nicaragua–northern Costa Rica shows a stronger *P* wave velocity anisotropy of 10% and a very clear arc-parallel orientation, that is independent of the different smoothing and grid parameters.

[46] In the vertical section (Figure 7), fast velocities are mostly aligned horizontally beneath the offshore areas down to 30 km depth. Like in central Costa Rica this finding can be seen as an indication that the fast velocity axis is predominantly horizontal and that the anisotropy is dominated by the LPO of olivine crystals in the subducting plate. This anisotropy pattern gets unclear between 30 and 100 km depth where the downgoing plate is bent. Then it switches back to horizontal at larger depth. This is surprising because one might expect to see the horizontal anisotropy orientation of the incoming slab turned to subvertical when the slab gets subducted with a 70° tilt. Indeed, we have to be very careful to interpret the anisotropy in these deep parts of the sections because the anisotropy resolution gets increasingly lower with depth. However, tentatively, we can regard these orientation changes as an indication that the LPO anisotropy prevalent at the shallow levels of the oceanic plate could be overprinted or deformed by concurring, more horizontal creep patterns, for example, along the planes of(reactivated bending-related faults. In the onshore areas of the overriding plate, especially beneath the volcanic arc, we observe a subvertical anisotropy. This could be explained by a structural anisotropy caused by arc-parallel systems of feeder dykes along which of melts and fluids propagate to the volcanoes. In this case the anisotropy would result the long-wavelength limit of average elastic constants of the "interlayering" of vertical rock sheets with high and low shear moduli corresponding to solid host rock and magma filled dykes. Similar features were found beneath the Merapi and Lawu volcanoes in Indonesia [*Koulakov et al.*, 2009].

4.4. Synthetic Modeling

[47] In order to determine the optimum values of the constraining inversion parameters and to estimate the resolution of the resulting models we performed a series of synthetic tests for both investigation areas. The resolution of the isotropic model of central Costa Rica (SE area) was thoroughly investigated in previous studies by *Dinc et al.* [2010] and *Koulakov* [2009]. It was found that this data set is capable of resolving horizontal fine structure near the 15 km scale. The vertical resolution is poorer (20–30 km scale), but still reasonable. Here we concentrate on testing the capacity of the algorithm to reconstruct the anisotropic patterns at coarse scales of several 10 km only.

[48] Figure 8 shows two synthetic tests for the central Costa Rica area. In the first case, we define a checkerboard model with periodic patterns of 50 km size. In "blue" blocks we define horizontal maximum and minimum velocities as anomalies of 15% and 5%, respectively. The maximum horizontal velocity is oriented along 45° azimuth. In the vertical direction we define 7% anomaly. This model corresponds to 9% of isotropic anomaly and 10% of horizontal anisotropy. In the "red" blocks the horizontal maximum, minimum and vertical velocity anomalies are −5%, −15% and −7%, respectively; the azimuthal orientation of the maximum velocity is −45°. Synthetic traveltimes were computed using the same source-receiver pairs as in the case of real data inversion based on the anisotropic 3-D bending algorithm of ray tracing. The synthetic data were perturbed with random noise having a realistic statistical distribution and average deviations of 0.15 and 0.25 s for *P* and *S* data, respectively, which provides a similar variance reduction as in the real case. The inversion procedure was performed with the same parameters as the inversion of the real data. Actually, the complete processing sequence was the following: (1) a preliminary first inversion of the real data with trial

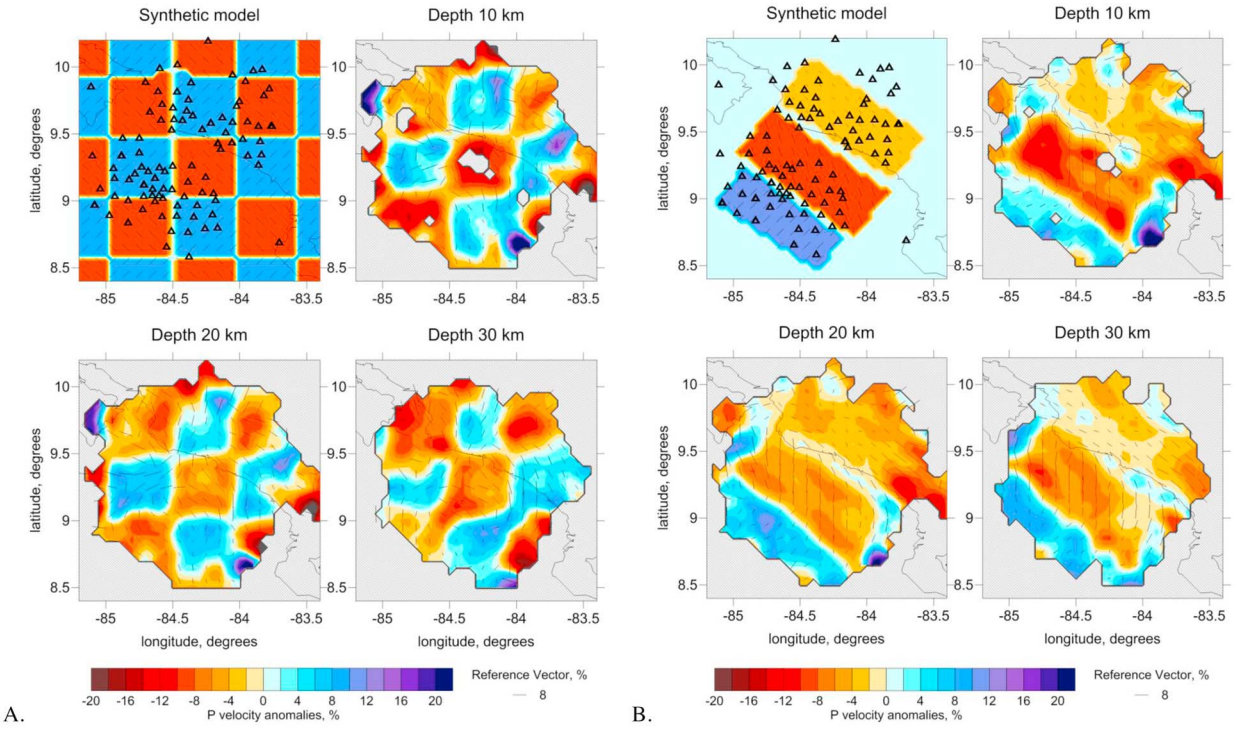

Figure 8. Synthetic tests for the SE area (central Costa Rica). (a) Checkerboard test with 50 km grid size. (b) Free-shaped anisotropic patterns. In both cases the models are unchanged with depth. Results are shown for 10, 20, and 30 km depths. The distribution of stations is shown in the plots with of the synthetic models.

processing parameters, (2) design of a synthetic model based on the first results in order to determine optimum values of the free steering parameters such as weights and damping coefficients, and (3) repeating of the real data inversion with the optimized parameters from step 2.

[49] The result of the checkerboard reconstruction for the central Costa Rica area is shown for three depth levels in Figure 8a. This test shows that the isotropic background structure is reconstructed robustly, but the quality of the anisotropic reconstructions is much poorer. In "red" blocks we recognize the NW-SE trending anisotropy, while in "blue" blocks the desired NE-SW orientation of anisotropy is much less clear. Note that a checkerboard model is not best suited for studying the anisotropy resolution because any periodic models appear to be effectively anisotropic due to geometrical effects. In this case, the anisotropic tomography cannot distinguish the "true" anisotropy from anisotropic artifacts caused by periodic structures.

[50] In this sense the second model with free-shaped patterns presented in Figure 8b is more appropriate for testing the anisotropy distribution observed in the real case. The synthetic model consists of three patterns (one with positive and two with negative isotropic anomalies). The anisotropy gradually changes the direction from SW-NE to SE-NW when passing from the offshore to onshore areas. This roughly represents the structure observed in real data inversion. The noise and other conditions for the inversion were the same as described in the previous paragraph for the checkerboard test. The reconstruction results presented for three depth levels show that the anisotropy orientation is robustly reconstructed based on the existing data. However, the reconstruction quality in the onshore area in the southern part of the model is poorer; thus the corresponding results should be interpreted only carefully.

[51] Examples of trials for searching an optimum set of inversion parameters are shown in Figure 9 corresponding to the synthetic model of Figure 8b. The most important parameters for anisotropic inversion are the following: (1) smoothing of the isotropic background model (parameter "Isotropic Wsm" in Figure 9), (2) damping of the amplitude of the isotropic background velocity perturbation ("Isotropic

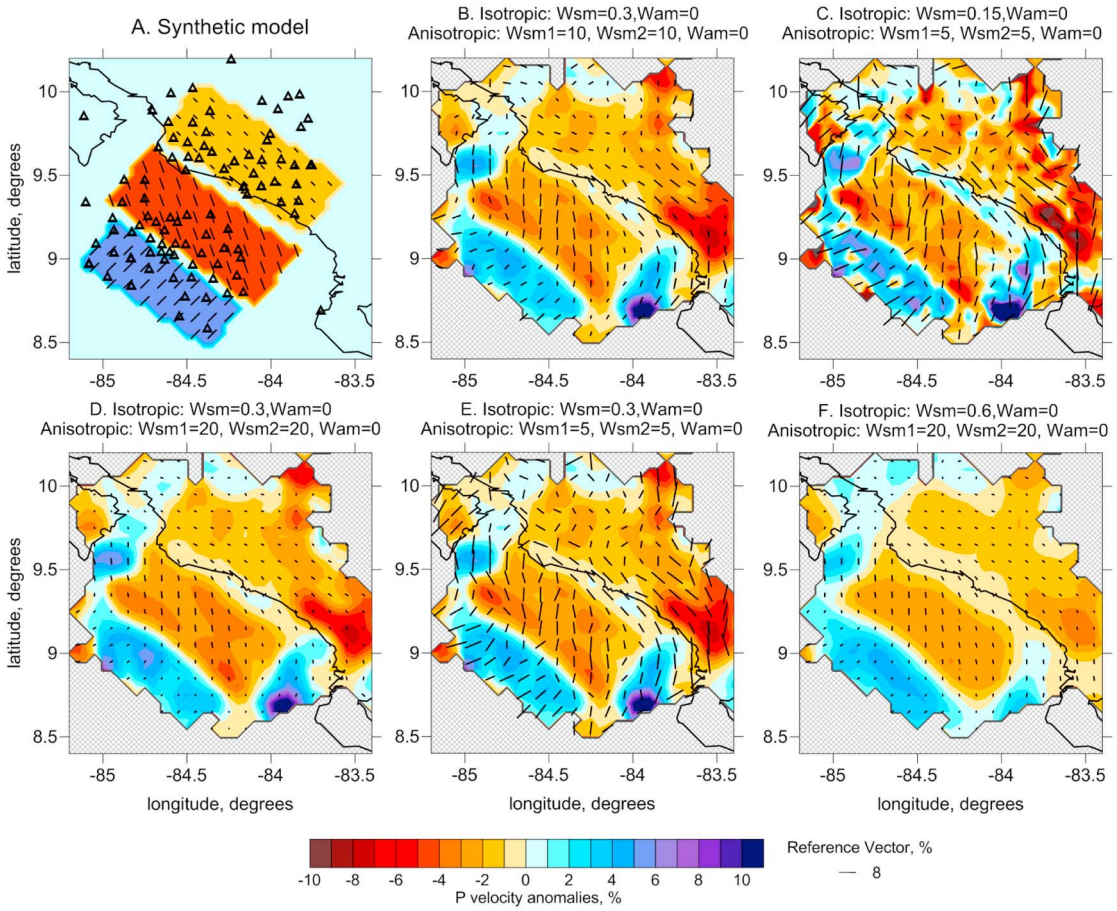

Figure 9. Reconstruction of the synthetic model for the Costa Rican data set with different parameters of isotropic and anisotropic damping. (a) The synthetic model (same as shown in Figure 8b). (b–f) Results for the depth of 15 km with different damping parameters as indicated above each plot. Figure 9b is the optimum model. Its parameters were used for the field data inversion of the Costa Rican data set.

Wam"), (3) spatial smoothing of the anisotropic parameters applied separately to each of the four anisotropic parameters ("Anisotropic Wsm1"), (4) damping of the difference between all pairs of anisotropic velocity components in each cell ("Anisotropic Wsm2"), and (5) damping of the size of the anisotropic velocity components ("Anisotropic Wam").

[52] In this study we did not apply damping coefficients to the amplitudes of the isotropic velocity perturbation. Instead, we conditioned the inversion by three smoothing coefficients in the anisotropic parameters. The effect of this smoothing is shown in Figure 9: Too much smoothing of the anisotropic parameters can cause a decrease of anisotropy of the recovered model to values much lower than in the true model (Figure 9d); too small smoothing can lead to an instability of the anisotropy orientation (Figure 9e). Note that in both these cases the isotropic model almost does not change. When we change both isotropic and anisotropic smoothing parameters (Figures 9c and 9f), both isotropic background and anisotropic perturbation change considerably: for isotropic Wsm = 0.6, the model is too smooth, whereas for Wsm = 0.15 some artifacts appears in the reconstructed model. The optimum parameters correspond to the model in Figure 9b, which were used for the inversion of the Costa Rican field data. Similar synthetic tests were performed for the Nicaragua data, too.

[53] In Figure 10 we show tomographic reconstructions of synthetic models with checkerboard and free-shaped anomalies that were computed for the source-receiver distribution of the northern Costa Rica–southern Nicaragua data. The optimum inversion parameters for these tests were obtained after

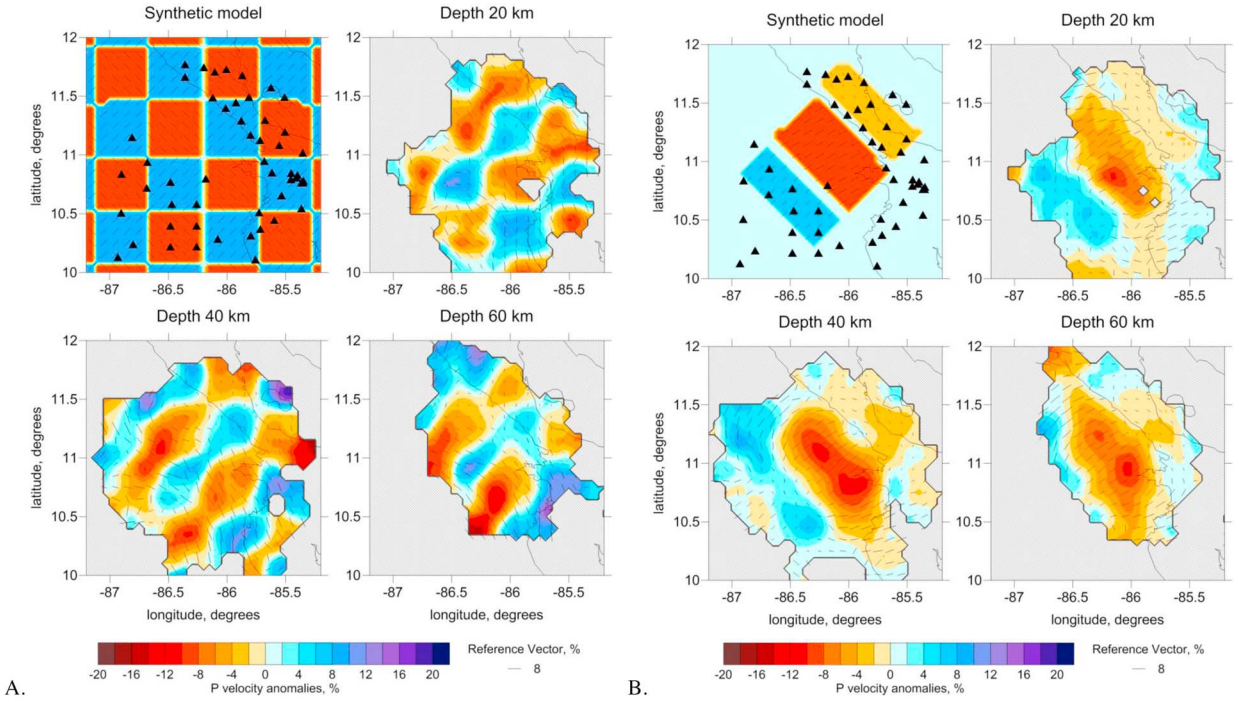

Figure 10. Synthetic tests for the NW area (northern Costa Rica and southern Nicaragua). (a) Checkerboard test with 50 km grid size. (b) Free-shaped anisotropic patterns. In both cases the models are unchanged with depth. The results are shown for 20, 40, and 60 km depths. The distribution of stations is shown in the plots with of the synthetic models.

several trials using the same procedure as described in previous paragraph. In general, these tests reveal the same features as for the central Costa Rica area, except for the different depth range. For the checkerboard model, the inversion reconstructs correctly the locations of isotropic anomalies, but the orientations of anisotropy in some places are not correct. Much better results for the anisotropy reconstruction are obtained for the second test that roughly represents the real situation. These synthetic tests provide more realistic information about the resolution capacity of the retrieved models and identifies features reliably that should be interpreted with prudence. The main conclusion coming from the synthetic testing is that the transition of the anisotropy orientation from trench-perpendicular offshore to trench-parallel onshore is a reliable feature.

[54] To investigate a possible trade-off between isotropic and anisotropic parameters, we have performed two tests which are presented in Figure 11. The source-receiver geometry corresponds to the Nicaragua–northern Costa Rica data set. In the first case (Figure 11, top) the synthetic traveltimes were computed for an isotropic model and then inverted using the anisotropic tomographic program. We see that the isotropic anomalies are resolved correctly, but we obtain some artifacts of anisotropy, too. However, the magnitude of this artifact anisotropy (~2%) is much lower than what was obtained from the field data.

[55] In the second case (Figure 11, bottom) we consider a purely anisotropic model (10% anisotropy) superimposed on an isotropic background. In the tomographic reconstruction results the orientation of anisotropy is robustly resolved in the central and NE parts of the model. In SE part of the model, the ray coverage is poor leading to errors in the orientation of anisotropy. The magnitude of anisotropy is somewhat smaller than the input (8% instead of 10% in the center of the model) and some artifact isotropic anomalies appear in the tomographic results. The size of these artificial isotropic velocity anomalies is 2%–3% and, therefore, much lower than the field observations.

5. Discussion

[56] Our results show that the crust and upper mantle beneath the Costa Rica and Nicaragua

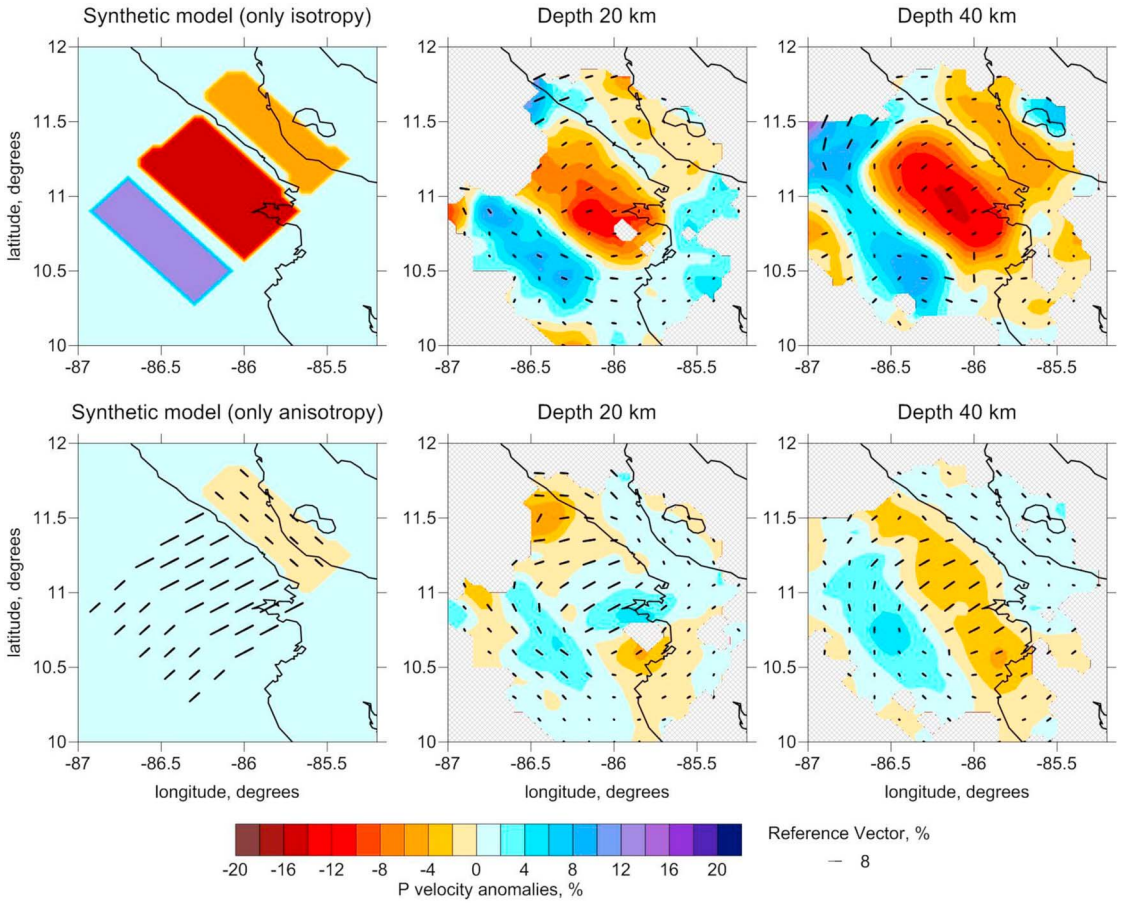

Figure 11. Test of trade-off between the isotropic and anisotropic parameters for the Nicaragua source-receiver geometry. (top) An isotropic version of the model of Figure 10 and its tomographic reconstruction based on the anisotropic algorithm. (bottom) Results for a model that contains only anisotropy.

segments of the Central America subduction zone appear to be strongly anisotropic. We found magnitudes of *P* wave velocity anisotropy of up to 8%–12%. However, these values should be interpreted with prudence because increasing the damping coefficients of the inversion causes a considerable decrease of the amplitude without a considerable decay of the data fit (especially for the central Costa Rica area). Therefore we prefer to interpret these values only qualitatively.

[57] In all trial and final runs of the inversion the subducting plate turned out to be anisotropic at all depth levels. The direction of fast velocity in the incoming oceanic plate fits to the direction of plate movement in both map view and vertical sections. The anisotropic properties of the incoming plate are compatible with LPO anisotropy of peridotite that was gradually formed during cooling of the oceanic floor when moving from a spreading center to the subduction zone (Figure 12). The idea that simultaneous cooling and moving of the lithosphere causes a preferential orientation of crystals parallel to the plate displacement has been established already in the 1960s [e.g., *Hess*, 1964; *Raitt et al.*, 1969]. Similar anisotropy patterns in the oceanic lithosphere were previously found in different studies, for example, in active source experiments by *Shimamura et al.* [1983] and in the eastern Pacific as part of a global model of lithosphere anisotropy [*Debayle et al.*, 2005]. For the Pacific Ocean comparable observations were compiled by different authors, too [e.g., *Smith et al.*, 2004; *Maggi et al.*, 2006].

[58] In the subducting part of the plate, the anisotropy patterns appear more complicated. In the vertical sections of southern Nicaragua–northern Costa Rica we observe strong variations of anisotropy at levels deeper than 30 km. Here the anisotropy pattern turns from subhorizontal in the offshore area to subvertical (30–100 km) and then back to

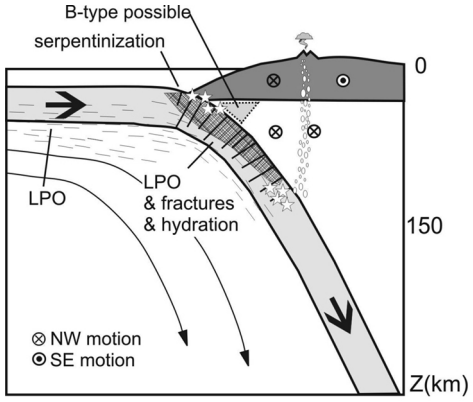

Figure 12. Schematic diagram showing the possible causes of anisotropy in the oceanic and overriding plates. Thin bars indicate LPO anisotropy in the oceanic asthenosphere and lithosphere reoriented toward plate motion. Thick lines represent the faults appearing in the bending part of the subducting plate, which can modify or overprint LPO anisotropy. The hatched area shows a zone of sepentinization (hydration) in the slab. Circles beneath the volcanic arc schematically represent slab fluids and melts ascending from the subducting slab. The melts can form arc-parallel melt bands (dykes) causing arc-parallel oriented azimuthal anisotropy. Out-of-plane arrows indicate mantle flow to the NW and regional dextral shear movement of the crust inferred from GPS measurements [*DeMets*, 2001]. The gray triangle in the outermost corner of the mantle wedge shows the small area in which B-type fabric could develop.

subhorizontal (100–200 km). A tentative interpretation of this behavior is that the anisotropy of the downgoing plate is influenced by bending-related faulting and deformation in addition to LPO at these depths (Figure 11). In addition, strong hydration of the oceanic lithosphere due to serpentinization in the upper part of the subduction zone may also contribute to perturbing the LPO anisotropy. However, to prove this, a different inversion approach would have to be applied that allows a free dip of the velocity ellipsoid.

[59] In the horizontal sections corresponding to the crust and uppermost mantle of the overriding plate beneath central Costa Rica (SE area) we observe a clear separation of different anisotropic domains (Figure 4). In the upper crust (<10 km depth) the anisotropic properties seem to be very variable on small scales and relatively weak. In the relatively small area of the central Costa Rica Deformation Belt (CCRDB between the trench and the volcano chain in Figure 1) all directions of fast velocities coexist, whereas trench-parallel orientations are found onshore outside the CCRDB in the SE. We regard this as an indicator of a tectonically complex crustal structure in the fore arc, the anisotropy of which is governed by the local fault setting. This view is supported by the mosaic structure of the isotropic velocity anomalies and even more by the tectonic maps of the region [e.g., *Denyer et al.*, 2003]. The low amplitude of anisotropy could also be explained by insufficient resolution: The checkerboard test shows that the tomographic inversion cannot map abrupt changes of anisotropy in separate blocks if their size is too small. We suppose that the anisotropy in the upper crust can be associated with a structure of crustal blocks and fault zones at scales smaller than the block size of the inversion. For the deeper sections of central Costa Rica, the horizontal orientation of fast velocity axes seems to be fairly regular. In the uppermost mantle of the overriding plate (30 km depth) the anisotropy is oriented subparallel to the trench and arc and roughly perpendicular to the direction of subduction. At depths larger than 30 km, the anisotropy remains arc-parallel only in the SE but turns to the E-W direction beneath the CCRDB in the NW of the study area. Since this orientation correlates with the extent direction of the CCRDB we tend to assume that both features are an expression of heterogeneity of lithospheric structure and related stress changes. However, one has to keep in mind that the anisotropy direction may be biased locally by velocity heterogeneity, too. This is evident from the checkerboard test in Figure 8. The more reliable information lies in the trend of anisotropy at scales of some 10 km.

[60] For the southern Nicaragua–northern Costa Rica area (Figure 6), a clear segmentation between the trench-perpendicular anisotropy of the incoming plate and trench-parallel anisotropy in the overriding plate and mantle wedge is observed in all depths. Only the anisotropy of the uppermost crust (depth <10 km) could not be determined because the recording stations were spaced too widely.

[61] The most important finding of our study is the observation that the fast axis of the *P* wave velocity of the upper mantle of the overriding plate is oriented nearly parallel to the arc along the 400 km long segment of the subduction zone that extends between southern Nicaragua and the NW part of the Talamanca collisional range in central Costa Rica. This result is compatible with the results from shear wave splitting of local and teleseismic arrivals that were observed in northern Costa Rica and Nicaragua [*Abt et al.*, 2009, 2010]. *Abt et al.* [2010] showed that the zone of arc-parallel anisotropy

seen in *SKS* splitting extends up to 200 km into the back arc of Nicaragua. However, splitting times decrease toward the Caribbean coast to about half of what is observed in the fore arc. Since the splitting of local *S* phases is about half of the *SKS* splitting it can be concluded that the arc-parallel anisotropic zone extents beneath the slab into deeper levels of the upper mantle.

[62] As discussed in the introduction of this paper, this sort of anisotropy can be interpreted in various ways. Several scenarios can be defined depending on whether an A type or B type of olivine fabric is assumed and on other factors:

[63] 1. A-type fabric would be associated with trench- or arc-parallel shear deformation or flow of either a dry peridotite, or a H_2O rich peridotite under high-temperature and low–shear stress conditions [e.g., *Zhang and Karato*, 1995; *Karato et al.*, 2008], that is where the combination of temperature T and shear stress τ follows τ (MPa) $< 0.8 \cdot$ T(°C)–640 order of magnitude.

[64] 2. B-type fabric would have to be associated with a H_2O rich mantle and regular corner flow perpendicular to the arc [e.g., *Jung and Karato*, 2001]. It would develop in those parts of the fore arc where temperatures are low or shear stresses high [e.g., *Lassak et al.*, 2006; *Katayama and Karato*, 2006; *Kneller et al.*, 2007; *Karato et al.*, 2008, and references therein], that is where the combination of temperature T and shear stress τ follows τ (MPa) $> 0.8 \cdot$ T(°C)–640 order of magnitude.

[65] 3. A third scenario can be seen in the rise of melt into the mantle along arc-parallel dykes leading to structure with a preferred orientation (SPO) that could create an effective azimuthal anisotropy. The orientation of this anisotropy would depend mainly on the preferred orientation of the dykes but would be nearly independent of the type olivine fabric because of the strong contrast in the shear moduli of melt and unmelted host rock.

[66] 4. Finally, downward flow of lower crustal material from beneath the arc into the upper mantle has to be considered as a contribution to SPO and LPO anisotropy [*Behn et al.*, 2007].

[67] Scenarios 1–4 describe possible causes of arc-parallel anisotropy that are located in the mantle wedge of the overriding plate. Regarding the splitting of *SKS* waves *Faccenda et al.* [2008] suggested that the downgoing plate could contribute to trench-parallel anisotropy, too, if it is permeated by serpentinized bend faults. Based on *Ranero et al.* [2003], *Faccenda et al.* [2008] assume that these faults are originally oblique at the outer rise and can get vertically oriented when the incoming plate dives downward. The resulting anisotropy of the downgoing part of the plate could not be distinguished from trench-parallel mantle wedge anisotropy because *SKS* wave splitting is an integral effect gathered all along the raypath. In contrast, the anisotropic *P* wave tomography applied in our study is capable to determine the portions of mantle wedge and slab anisotropy separately. Although the resolution is low it can be concluded that the anisotropy of the downgoing plate is not uniform and not predominantly subvertical.

[68] The mantle wedge scenarios 1–3 were discussed in detail by *Abt et al.* [2009] with respect to the situation in Nicaragua and northern Costa Rica. In order to get a further indication which of the options is the most likely for the explanation of the *P* wave anisotropy pattern of the mantle wedge, the following two key observations have to be considered in addition:

[69] 1. The deformation of the upper plate as measured by GPS and corresponding modeling show that the upper crust of Costa Rica and Nicaragua follows an escape movement to the northwest that originates at or near the area where the Cocos Ridge collides with the Caribbean Plate [*LaFemina et al.*, 2009; *Correa-Mora et al.*, 2009; *Turner et al.*, 2007]. In Nicaragua the escape movement seems to correspond to a dextral strike-slip movement along the volcanic arc with an arc-parallel relative displacement of ~14 mm/yr [*DeMets*, 2001]. This strike-slip movement could be recorded in Costa Rica, too, but with decreasing displacement toward SE where 8 mm/yr was recorded in the Nicoya region and no strike-slip motion in the Osa region [*Lundgren et al.*, 1999; *Norabuena et al.*, 2004]. However, regarding the slip localization the situation is more complicated in Costa Rica than in Nicaragua. Numerous NW-SE oriented faults have been identified (see the tectonic atlas of *Denyer et al.* [2003]), some of them strike-slip, but they seem to form a complicated diffuse fault system rather than a localized strike-slip fault. This applies especially to the Central Costa Rica Deformation Belt. The cause of this large-scale escape movement can be seen in three processes: (1) in the Cocos Ridge collision and the formation of convergent structure in southern Costa Rica [e.g., *Quintero and Güendel*, 2000; *Fisher et al.*, 2004; *Dinc et al.*, 2010], (2) in a complementary extensional regime in Nicaragua

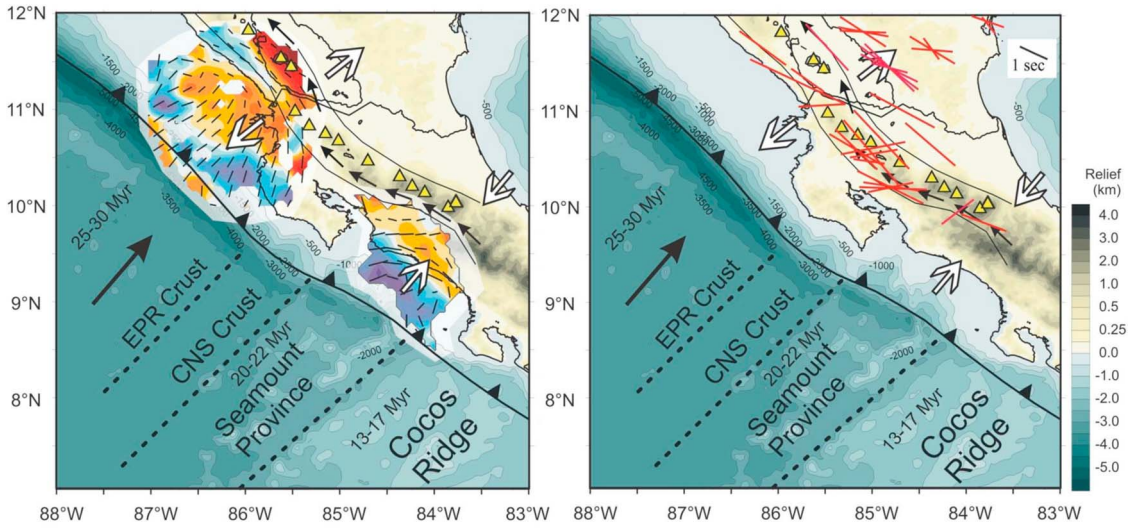

Figure 13. (left) Variation of average isotropic *P* wave velocity and orientation of the axis of fast *P* wave velocity at 50 km depth in the upper mantle of southern Nicaragua and Costa Rica (compare Figures 4 and 6) with a sketch of trench-parallel flow (dark solid lines and arrows) in the mantle wedge. Yellow triangles are the active volcanoes. White arrows schematically indicate zones of compression and extension. EPR, East Pacific Rise; CNS, Cocos-Nazca Spreading Center. (right) *SKS* splitting observations in the same area [from *Abt et al.*, 2010]. The orientation and length of the red lines show the azimuth of the leading split *SKS* wave and the splitting time, respectively.

possibly originating from slab retreat (see white arrows in Figure 13 that schematically indicate zones of extension and compression), and (3) in the plate convergence angle which deviates ~10° counterclockwise from the orthogonal except in the southern part of the investigation area (Osa region).

[70] 2. Geochemical analysis [*Carr et al.*, 2007; *Hoernle et al.*, 2008] sees evidence for trench-parallel flow in the mantle wedge beneath Costa Rica and Nicaragua based on the observation of seamount signatures in Central American volcanoes. The isotopic signature of the Galapagos hot spot track, which originally comes in with the subducting plate along the Cocos Ridge, is observed also in volcanoes from central Costa Rica to northwestern Nicaragua, however in concentrations decreasing with distance from the Cocos Ridge. *Hoernle et al.* [2008] interpret this heterogeneity as an expression of mass transport and mixing. They determined the age of these isotopic signatures and estimated a rate of the northwestward flow as 63–190 mm/yr, a value that is comparable with the velocity of subducting Cocos plate motion (~80 mm/yr). The assumption of trench-parallel flow is supported by trench-parallel *S* wave anisotropy estimated from shear wave splitting in Nicaragua in the same study [*Hoernle et al.*, 2008].

[71] The geodetic and geochemical findings as well as the change in the regional stress system clearly indicate that a 2-D interpretation model of the observed *P* wave anisotropy is not favorable. Therefore, a 2-D corner flow (scenario 2) appears less likely than LPO caused by escape flow to the northwest (Figure 13).

[72] Planar feeder dykes parallel to the arc (scenario 3) cannot be excluded as a possible cause of the trench-parallel *P* wave anisotropy in general. They would occur beneath or near to the active volcanoes and could contribute to the anisotropy in Nicaragua and northern Costa Rica. However, in both study areas the trench-parallel anisotropy pattern is observed also remote from the arc: in Nicaragua up to 50 km into the fore arc and 200 km into the back arc, and in Costa Rica up to 100 km distance from Mount Irazu, the most eastern active volcano, into the fore arc. Therefore, we conclude that planar melt bands cannot be the exclusive cause of the observed *P* wave anisotropy. However, preferably oriented melt bands can contribute significantly to the anisotropy on a local scale. To get more insight into the possible role of melt bands the 3-D structure of the stress system has to be modeled.

[73] The same applies to a possible foundering of lower crustal material into the mantle (scenario 4) which would enhance arc-parallel anisotropy near

the arc but would show arc-normal components off the arc, at least at lower crustal levels. Since the overall pattern is arc-parallel it can be concluded that lower crustal foundering may contribute to the observed anisotropy but does not seem to be a the major cause.

[74] The incoming plate of Nicaragua and northern Costa Rica is considered to be significantly serpentinized [*Ranero et al.*, 2003; *Ivandic et al.*, 2010; *Linkimer et al.*, 2010]. The release of this water into the overriding mantle could create favorable conditions for the development of B-type fabric. However, estimates of the mantle temperatures in Central America [*Rüpke et al.*, 2002; *Peacock et al.*, 2005] show that the temperatures are likely to be too high for B-type fabric in most of the mantle wedge if shear stresses <100 MPa are assumed. An exception is only a small region at the outermost fore-arc corner (area indicated in Figure 12). Therefore, A-type LPO has to be favored for the major part of the mantle wedge of southern Nicaragua and Costa Rica. This implies at the same time that the escape movement is the more likely cause of the observed orientation of *P* wave anisotropy. In a setting of arc-parallel deformation B-type fabric would lead to arc-perpendicular anisotropy, which is not observed in the mantle wedge. In Costa Rica and southern Nicaragua, B-type fabric seems to be only a local factor spatially restricted to the outermost corner of the mantle wedge where it can hardly be distinguished from the anisotropy pattern of the incoming plate.

[75] Based on the arguments above, we propose that the most likely explanation for the observed azimuthal pattern of *P* wave anisotropy in the mantle wedge is a trench-parallel shear deformation and/or flow originating in the compressional zone at and around the Cocos Ridge collision area. This implies that the deformation of the upper crust expressed by GPS displacement field can be traced down to mantle depth. Since the anisotropic flow pattern is observed at the Moho level, too (see 40 and 30 km depth slices in Figures 4 and 6, respectively) it has to be considered that the lowermost ductile parts of the crust could be involved in the escape flow as well. The observation of arc-parallel anisotropy in *SKS* and their larger splitting times compared to local *S* phases indicate that deeper parts of the lithosphere and possibly the asthenosphere are involved in the flow or shearing, too [*Abt et al.*, 2010].

[76] It has been suggested that this possible asthenospheric flow might be part of a continent-scale flow system caused by the rollback of the Nazca Plate offshore South America. An alternative suggestion is to see it as back flow from a hypothetic slab tear-off located in southern Costa Rica or Panama [see *Abt et al.*, 2010, and references therein]. If this applied the mainstream of this long-distance flow would have to be located in the asthenosphere, that is, much deeper than the investigation depth of our study. The observed *P* wave anisotropy and underlying shear deformation would then have to be driven from depth by the asthenosphere through viscous coupling. However, these scenarios appear highly speculative at the present stage of seismological observations. In particular the transition from southern Costa Rica via Panama to the north of South America and the involvement of the Caribbean side are widely unclear. A recent receiver function study of the area of the northern Talamanca range, directly south of our investigation area, does not show evidence of a slab tear-off at depth shallower than ~100 km [*Dzierma et al.*, 2011].

6. Conclusions

[77] The main result of this study is the determination of the anisotropic *P* velocity structure in the crust and uppermost mantle beneath two separate areas in Central America that cover offshore and onshore segments of the Costa Rican and Nicaraguan subduction zones. In both investigation areas the incoming oceanic plate shows an anisotropy parallel to the movement of the plate that is clearly seen in both horizontal and vertical sections. We propose that this is related to LPO anisotropy of the peridotite that was gradually formed when the cooling oceanic plate moved from the spreading center to the subduction zone. In the subduction zone, the anisotropy features become more complex. Within the dipping slab we find evidence that the anisotropy varies from horizontal to vertical and then back to horizontal. This sort of behavior could be caused by bending-related faulting and hydration in the uppermost part of the subduction zone. Subhorizontal deformation or creep can occur along reactivated bend fault planes at depth where they have been turned to subhorizontal by the subduction The corresponding seismic anisotropy pattern could modify or even overprint the original anisotropy of the incoming plate. However, we have to emphasize that the anisotropy change along the slab is at the limits of resolution and that it needs more experimental efforts to confirm it.

[78] The most important and well resolved feature of our model is a clear segmentation of anisotropy in two major zones in map view. In the both study areas, we observe a change from the trench-perpendicular anisotropy of the incoming plate and to a trench-parallel one in the overriding plate and the onshore mantle wedge. We discussed several scenarios for such an along trench anisotropy. Based on joint consideration of our model together with results of GPS measurements, numerical modeling and geochemistry, the most plausible explanation for such anisotropy is an escape flow in the mantle wedge and, possibly, the lowermost crust oriented parallel to the arc. It could be caused by convergence in southern Costa Rica combined with transtension and extension in Nicaragua. The arc-parallel flow could be deviated by local lithospheric heterogeneity in the area of the Central Costa Rica Deformation Belt.

Acknowledgments

[79] This publication is contribution 199 of the Sonderforschungsbereich 574 "Volatiles and Fluids in Subduction Zones" at Kiel University. The Geophysical Instrument Pool GIPP of the Geoforschungszentrum Potsdam provided the short-period seismic stations. The work of Ivan Koulakov is supported by the Helmholtz Society and RFBR Joint Research Project 09-05-91321-SIG a, Multidisciplinary Projects SB RAS 21 and SB-UrO-DVORAS 96, and project ONZ RAS 7.4. We gratefully acknowledge the constructive criticism from T. Becker (Editor), the anonymous Associate Editor, and two anonymous reviewers that helped to improve the article.

References

Abt, D. L., and K. M. Fischer (2008), Resolving three-dimensional anisotropic structure with shear-wave splitting tomography, *Geophys. J. Int.*, *173*, 859–886, doi:10.1111/j.1365-246X.2008.03757.x.

Abt, D. L., K. M. Fischer, G. A. Abers, W. Strauch, J. M. Protti, and V. Gonzalez (2009), Shear wave anisotropy beneath Nicaragua and Costa Rica: Implications for flow in the mantle wedge, *Geochem. Geophys. Geosyst.*, *10*, Q05S15, doi:10.1029/2009GC002375.

Abt, D. L., K. M. Fischer, G. A. Abers, J. M. Protti, V. González, and W. Strauch (2010), Constraints on upper mantle anisotropy surrounding the Cocos slab from *SK(K)S* splitting, *J. Geophys. Res.*, *115*, B06316, doi:10.1029/2009JB006710.

Anderson, M. L., G. Zand, E. Triep, M. Fouch, and S. Beck (2004), Anisotropy and mantle flow in the Chile-Argentina subduction zone from shear wave splitting analysis, *Geophys. Res. Lett.*, *31*, L23608, doi:10.1029/2004GL020906.

Arroyo, I. G., S. Husen, E. R. Flueh, J. Gossler, E. Kissling, and G. E. Alvarado (2009), Three-dimensional *P* wave velocity structure on the shallow part of the Central Costa Rican Pacific margin from local earthquake tomography using off- and onshore networks, *Geophys. J. Int.*, *179*, 827–849, doi:10.1111/j.1365-246X.2009.04342.x.

Barckhausen, U., C. R. Ranero, R. von Huene, S. C. Cande, and H. A. Roeser (2001), Revised tectonic boundaries in the Cocos Plate off Costa Rica: Implications for the segmentation of the convergent margin and for plate tectonic models, *J. Geophys. Res.*, *106*, 19,207–19,220, doi:10.1029/2001JB000238.

Behn, M. D., G. Hirth, and P. B. Kelemen (2007), Trench-parallel anisotropy produced by foundering of arc lower crust, *Science*, *317*, 108–111, doi:10.1126/science.1141269.

Bialas, J., and E. R. Flueh (1999), Ocean bottom seismometers, *Sea Technol.*, *40*, 41–46.

Boschi, L., and A. M. Dziewonski (1999), High- and low-resolution images of the Earth's mantle: Implications of different approaches to tomographic modeling, *J. Geophys. Res.*, *104*, 25,567–25,594, doi:10.1029/1999JB900166.

Carr, M., M. D. Feigenson, L. C. Patino, and J. A. Walker (2003), Volcanism and geochemistry in Central America: Progress and problems, in *Inside the Subduction Factory*, *Geophys. Monogr. Ser.*, vol. 138, edited by J. Eiler, pp. 153–179, AGU, Washington, D. C.

Carr, M. J., I. Saginor, G. E. Alvarado, L. L. Bolge, F. N. Lindsay, K. Milidakis, B. D. Turrin, M. D. Feigenson, and C. C. Swisher (2007), Element fluxes from the volcanic front of Nicaragua and Costa Rica, *Geochem. Geophys. Geosyst.*, *8*, Q06001, doi:10.1029/2006GC001396.

Colombo, D., G. B. Cimini, and R. de Franco (1997), Three dimensional velocity structure of the upper mantle beneath Costa Rica from teleseismic tomography study, *Geophys. J. Int.*, *131*, 189–208.

Correa-Mora, F., C. DeMets, D. Alvarado, H. L. Turner, G. Mattioli, D. Hernandez, C. Pullinger, M. Rodriguez, and C. Tenorio (2009), GPS-derived coupling estimates for the Central America subduction zone and volcanic arc faults: El Salvador, Honduras and Nicaragua, *Geophys. J. Int.*, *179*, 1279–1291, doi:10.1111/j.1365-246X.2009.04371.x.

Debayle, E., B. Kennett, and K. Priestley (2005), Global azimuthal seismic anisotropy and the unique plate-motion deformation of Australia, *Nature*, *433*, 509–512, doi:10.1038/nature03247.

DeMets, C. (2001), A new estimate for present-day Cocos-Caribbean Plate motion: Implications for slip along the Central American Volcanic Arc, *Geophys. Res. Lett.*, *28*, 4043–4046, doi:10.1029/2001GL013518.

DeMets, C., R. G. Gordon, D. F. Argus, and S. Stein (1994), Effect of recent revisions to the geomagnetic reversal timescale on estimates of current plate motions, *Geophys. Res. Lett.*, *21*, 2191–2194, doi:10.1029/94GL02118.

Denyer, P., W. Montero, and G. E. Alvarado (2003), *Atlas tectonico de Costa Rica*, 79 pp., Ed. de la Univ. de Costa Rica, San José.

Dinc, A. N., I. Koulakov, M. Thorwart, W. Rabbel, E. R. Flueh, I. Arroyo, W. Taylor, and G. Alvarado (2010), Local earthquake tomography of central Costa Rica: Transition from seamount to ridge subduction, *Geophys. J. Int.*, *183*, 286–302, doi:10.1111/j.1365-246X.2010.04717.x.

Dinc, A. N., W. Rabbel, E. Flueh, and W. Taylor (2011), Mantle Wedge Hydration in Nicaragua from Local Earthquake Tomography, *Geophys. J. Int.*, doi:10.1111/j.1365-246X.2011.05041.x, in press.

Dzierma, Y., W. Rabbel, M. M. Thorwart, E. R. Flueh, M. M. Mora, and G. E. Alvarado (2011), The steeply subducting edge of the Cocos Ridge: Evidence from receiver functions beneath the northern Talamanca Range, south-

central Costa Rica, *Geochem. Geophys. Geosyst.*, *12*, Q04S30, doi:10.1029/2010GC003477.

Faccenda, M., L. Burlini, T. V. Gerya, and D. Mainprice (2008), Fault-induced seismic anisotropy by hydration in subducting oceanic plates, *Nature*, *455*, 1097–1100, doi:10.1038/nature07376.

Fisher, D. M., T. W. Gardner, and P. Sak (2004), Active thrusting in the inner fore arc of an erosive convergent margin, Pacific coast, Costa Rica, *Tectonics*, *23*, TC2007, doi:10.1029/2002TC001464.

Gardner, T. W., D. Verdonck, and N. M. Pinter (1992), Quaternary uplift astride the aseismic Cocos Ridge, Pacific coast, Costa Rica, *Geol. Soc. Am. Bull.*, *104*, 219–232, doi:10.1130/0016-7606(1992)104<0219:QUATAC>2.3.CO;2.

Gräfe, K. (1998), Exhumation and thermal evolution of the Cordillera de Talamanca (Costa Rica): Constraints from fission track analysis, ^{40}Ar-^{39}Ar and ^{87}Rb-^{87}Sr chronology, Ph.D. thesis, Univ. Tübingen, Tübingen, Germany.

Hauff, F., K. Hoernle, H. U. Schmincke, and R. Werner (1997), A Mid Cretaceous origin for the Galapagos hotspot: Volcanological, petrological and geochemical evidence from Costa Rican oceanic crustal segments, *Int. J. Earth Sci.*, *86*, 141–155.

Hess, H. (1964), Seismic anisotropy of the upper mantle under oceans, *Nature*, *203*, 629–631, doi:10.1038/203629a0.

Hoernle, K., and F. Hauff (2007), Oceanic igneous complexes in Central America, in *Central America: Geology, Resources and Hazards*, edited by J. Bundschuh and G. Alvarado, pp. 523–548, Taylor and Francis, London.

Hoernle, K., D. L. Abt, K. M. Fischer, H. Nichols, F. Hauff, G. Abers, P. van den Bogaard, G. Alvarado, M. Protti, and W. Strauch (2008), Geochemical and geophysical evidence for arc-parallel flow in the mantle wedge beneath Costa Rica and Nicaragua, *Nature*, *451*, 1094–1097, doi:10.1038/nature06550.

Holtzman, B. K., D. L. Kohlstedt, M. E. Zimmerman, F. Heidelbach, T. Hiraga, and J. Hustoft (2003), Melt segregation and strain partitioning: Implications for seismic anisotropy and mantle flow, *Science*, *301*, 1227–1230, doi:10.1126/science.1087132.

Husen, S., R. Quintero, E. Kissling, and B. Hacker (2003), Subduction-zone structure and magmatic processes beneath Costa Rica constrained by local earthquake tomography and petrological modelling, *Geophys. J. Int.*, *155*, 11–32, doi:10.1046/j.1365-246X.2003.01984.x.

Ivandic, M., I. Grevemeyer, J. Bialas, and C. J. Petersen (2010), Serpentinization in the trench-outer rise region offshore of Nicaragua: Constraints from seismic refraction and wide-angle data, *Geophys. J. Int.*, *180*, 1253–1264, doi:10.1111/j.1365-246X.2009.04474.x.

Jung, H., and S. Karato (2001), Water-induced fabric transitions in olivine, *Science*, *293*, 1460–1463, doi:10.1126/science.1062235.

Karato, S., H. Jung, I. Katayama, and P. Skemer (2008), Geodynamic significance of seismic anisotropy of the upper mantle: New insights from laboratory studies, *Annu. Rev. Earth Planet. Sci.*, *36*, 59–95, doi:10.1146/annurev.earth.36.031207.124120.

Katayama, I., and S. Karato (2006), Effects of temperature on the B- to C-type fabric transition in olivine, *Phys. Earth Planet. Inter.*, *157*, 33–45, doi:10.1016/j.pepi.2006.03.005.

Kissling, E., W. Ellsworth, D. Eberhart-Phillips, and U. Kradolfer (1994), Initial reference models in local earthquake tomography, *J. Geophys. Res.*, *99*, 19,635–19,646, doi:10.1029/93JB03138.

Kneller, E. A., and P. E. van Keken (2007), Trench-parallel flow and seismic anisotropy in the Mariana and Andean subduction systems, *Nature*, *450*, 1222–1225, doi:10.1038/nature06429.

Kneller, E. A., P. E. van Keken, I. Katayama, and S. Karato (2007), Stress, strain, and B-type olivine fabric in the fore-arc mantle: Sensitivity tests using high-resolution steady-state subduction zone models, *J. Geophys. Res.*, *112*, B04406, doi:10.1029/2006JB004544.

Koulakov, I. (2009), LOTOS code for local earthquake tomographic inversion. Benchmarks for testing tomographic algorithms, *Bull. Seismol. Soc. Am.*, *99*, 194–214, doi:10.1785/0120080013.

Koulakov, I., A. Jakovlev, and B. G. Luehr (2009), Anisotropic structure beneath central Java from local earthquake tomography, *Geochem. Geophys. Geosyst.*, *10*, Q02011, doi:10.1029/2008GC002109.

Kutterolf, S., A. Freundt, and W. Peréz (2008), Pacific offshore record of plinian arc volcanism in Central America: 2. Tephra volumes and erupted masses, *Geochem. Geophys. Geosyst.*, *9*, Q02S02, doi:10.1029/2007GC001791.

LaFemina, P., T. H. Dixon, R. Govers, E. Norabuena, H. Turner, A. Saballos, G. Mattioli, M. Protti, and W. Strauch (2009), Fore-arc motion and Cocos Ridge collision in Central America, *Geochem. Geophys. Geosyst.*, *10*, Q05S14, doi:10.1029/2008GC002181.

Lassak, T. M., M. J. Fouch, C. E. Hall, and E. Kaminski (2006), Seismic characterization of mantle flow in subduction systems: Can we resolve a hydrated mantle wedge?, *Earth Planet. Sci. Lett.*, *243*, 632–649, doi:10.1016/j.epsl.2006.01.022.

Linkimer, L., S. L. Beck, S. Y. Schwartz, G. Zandt, and V. Levin (2010), Nature of crustal terranes and the Moho in northern Costa Rica from receiver function analysis, *Geochem. Geophys. Geosyst.*, *11*, Q01S19, doi:10.1029/2009GC002795.

Long, M., and T. Becker (2010), Mantle dynamics and seismic anisotropy, *Earth Planet. Sci. Lett.*, *297*, 341–354, doi:10.1016/j.epsl.2010.06.036.

Lundgren, P., M. Protti, A. Donnellan, M. Heflin, E. Hernandez, and D. Jefferson (1999), Seismic cycle and plate margin deformation in Costa Rica: GPS observations from 1994 to 1997, *J. Geophys. Res.*, *104*(B12), 28,915–28,926, doi:10.1029/1999JB900283.

Maggi, A., E. Debayle, K. Priestley, and G. Barruol (2006), Azimuthal anisotropy of the Pacific region, *Earth Planet. Sci. Lett.*, *250*, 53–71, doi:10.1016/j.epsl.2006.07.010.

Norabuena, E., et al. (2004), Geodetic and seismic constraints on some seismogenic zone processes in Costa Rica, *J. Geophys. Res.*, *109*, B11403, doi:10.1029/2003JB002931.

Paige, C. C., and M. A. Saunders (1982), LSQR: An algorithm for sparse linear equations and sparse least squares, *Trans. Math. Software*, *8*, 43–71, doi:10.1145/355984.355989.

Peacock, S. M., P. E. van Keken, S. D. Holloway, B. R. Hacker, G. A. Abers, and R. L. Fergason (2005), Thermal structure of the Costa Rica–Nicaragua subduction zone, *Phys. Earth Planet. Inter.*, *149*, 187–200, doi:10.1016/j.pepi.2004.08.030.

Protti, M., S. Y. Schwartz, and G. Zandt (1999), Simultaneous inversion for earthquake location and velocity structure beneath central Costa Rica, *Bull. Seismol. Soc. Am.*, *86*, 19–31.

Quintero, R., and F. Güendel (2000), Stress field in Costa Rica, Central America, *J. Seismol.*, *4*, 297–319, doi:10.1023/A:1009867405248.

Quintero, R., and E. Kissling (2001), An improved *P* wave velocity reference model for Costa Rica, *Geophys. J. Int.*, *40*, 3–19.

Rabbel, W., and W. D. Mooney (1996), Seismic anisotropy of the crystalline crust: What does it tell us?, *Terra Nova*, *8*, 16–21, doi:10.1111/j.1365-3121.1996.tb00721.x.

Raitt, R. W., G. Shor, G. Morris, and H. Kirk (1969), Anisotropy of the Pacific upper mantle, *J. Geophys. Res.*, *74*, 3095–3109, doi:10.1029/JB074i012p03095.

Ranero, C. R., J. Phipps Morgan, K. D. McIntosh, and C. Reichert (2003), Bending, faulting, and mantle serpentinization at the Middle America trench, *Nature*, *425*, 367–373, doi:10.1038/nature01961.

Rüpke, L. H., J. Phipps Morgan, M. Hort, and J. A. D. Connolly (2002), Are the regional variations in Central American arc lavas due to differing basaltic versus peridotitic slab sources of fluids?, *Geology*, *30*, 1035–1038, doi:10.1130/0091-7613(2002)030<1035:ATRVIC>2.0.CO;2.

Russo, R. M., and P. G. Silver (1994), Trench-parallel flow beneath the Nazca plate from seismic anisotropy, *Science*, *263*, 1105–1111, doi:10.1126/science.263.5150.1105.

Sadofsky, S. J., M. Portnyagin, K. Hoernle, and P. van den Bogaard (2008), Subduction cycling of volatiles and trace elements through the Central American volcanic arc: Evidence from melt inclusions, *Contrib. Mineral. Petrol.*, *155*, 433–456, doi:10.1007/s00410-007-0251-3.

Sallarès, V., and P. Charvis (2003), Crustal thickness constraints on the geodynamic evolution of the Galapagos Volcanic Province, *Earth Planet. Sci. Lett.*, *214*, 545–559, doi:10.1016/S0012-821X(03)00373-X.

Sallarès, V., J. J. Danobeitia, and E. R. Flueh (2000), Seismic tomography with local earthquakes in Costa Rica, *Tectonophysics*, *329*, 61–78, doi:10.1016/S0040-1951(00)00188-8.

Sallarès, V., P. Charvis, E. R. Flueh, and J. Bialas (2005), Seismic structure of the Carnegie ridge and the nature of the Galapagos hotspot, *Geophys. J. Int.*, *161*, 763–788, doi:10.1111/j.1365-246X.2005.02592.x.

Savage, M. K. (1999), Seismic anisotropy and mantle deformation: What have we learned from shear wave splitting?, *Rev. Geophys.*, *37*, 65–106, doi:10.1029/98RG02075.

Shimamura, H., T. Asada, K. Suyehiro, T. Yamada, and H. Inatani (1983), Longshot experiments to study velocity anisotropy in the oceanic lithosphere of the northwestern Pacific, *Phys. Earth Planet. Inter.*, *31*, 348–362, doi:10.1016/0031-9201(83)90094-8.

Smith, D. B., M. H. Ritzwoller, and N. M. Shapiro (2004), Stratification of anisotropy in the Pacific upper mantle, *J. Geophys. Res.*, *109*, B11309, doi:10.1029/2004JB003200.

Turner, H. L. I., P. LaFemina, A. Saballos, G. S. Mattioli, P. E. Jansma, and T. Dixon (2007), Kinematics of the Nicaraguan forearc from GPS geodesy, *Geophys. Res. Lett.*, *34*, L02302, doi:10.1029/2006GL027586.

van der Sluis, A., and H. A. van der Vorst (1987), Numerical solution of large, sparse linear algebraic systems arising from tomographic problems, in *Seismic Tomography*, edited by G. Nolet, pp. 49–83, D. Reidel, Dordrecht, Netherlands.

von Huene, R., J. Hoffmann, P. Holler, R. Leon, O. Barrios, J. Chavarría, J. Jeschke, and D. Escobedo (1995), Morphotectonics of the Pacific convergent margin of Costa Rica, *Spec. Pap. Geol. Soc. Am.*, *295*, 291–307.

von Huene, R., C. R. Ranero, W. Weinrebe, and K. Hinz (2000), Quaternary convergent margin tectonics of Costa Rica, segmentation of the Cocos Plate, and central American volcanism, *Tectonics*, *19*, 314–334, doi:10.1029/1999TC001143.

Walther, C. H. E. (2003), The crustal structure of the Cocos ridge off Costa Rica, *J. Geophys. Res.*, *108*(B3), 2136, doi:10.1029/2001JB000888.

Walther, C., and E. R. Flueh (2002), Remnant of the ancient Farallon Plate breakup: A low-velocity body in the lower oceanic crust off Nicoya Peninsula, Costa Rica - evidence from wide-angle seismics, *Geophys. Res. Lett.*, *29*(19), 1939, doi:10.1029/2002GL015026.

Werner, R., K. Hoernle, P. van den Bogaard, C. Ranero, R. von Huene, and D. Korich (1999), Drowned 14-m.y.-old Galapagos archipelago off the coast of Costa Rica: Implications for tectonic and evolutionary models, *Geology*, *27*, 499–502, doi:10.1130/0091-7613(1999)027<0499:DMYOGP>2.3.CO;2.

Wilson, D. S., D. A. Teagle, and G. D. Acton (2003), First results from Hole 1256D—A new ocean-crust reference hole drilled in fast-spread crust during ODP Leg 206, *Eos Trans. AGU*, *84*(46), Fall Meet. Suppl., Abstract U12A-02.

Yao, Z. S., R. Quintero, and R. G. Roberts (1999), Tomographic imaging of *P*- and *S*-wave velocity structure beneath Costa Rica, *J. Seismol.*, *3*, 177–190, doi:10.1023/A:1009885321799.

Zhang, S., and S. Karato (1995), Lattice preferred orientation of olivine aggregates deformed in simple shear, *Nature*, *375*, 774–777, doi:10.1038/375774a0.